NASA/TP–20260003940

Thermal Considerations for 2039 Opposition Class Nuclear Electric Propulsion/Chemical Propulsion Crewed Mars Mission

Tai Lily Valdés
Langley Research Center, Engineering Directorate, Structural and Thermal Systems Branch [Hampton, VA]

Will J. Grier, Amanda E. Stark
Langley Research Center, Engineering Directorate, Structural and Thermal Systems Branch [Hampton, VA]

May 2026

NASA STI Program Report Series

Since its founding, NASA has been dedicated to the advancement of aeronautics and space science. The NASA scientific and technical information (STI) program plays a key part in helping NASA maintain this important role.

The NASA STI program operates under the auspices of the Agency Chief Information Officer. It collects, organizes, provides for archiving, and disseminates NASA's STI. The NASA STI program provides access to the NTRS Registered and its public interface, the NASA Technical Reports Server, thus providing one of the largest collections of aeronautical and space science STI in the world. Results are published in both non-NASA channels and by NASA in the NASA STI Report Series, which includes the following report types:

- TECHNICAL PUBLICATION. Reports of completed research or a major significant phase of research that present the results of NASA Programs and include extensive data or theoretical analysis. Includes compilations of significant scientific and technical data and information deemed to be of continuing reference value. NASA counterpart of peer-reviewed formal professional papers but has less stringent limitations on manuscript length and extent of graphic presentations.

- TECHNICAL MEMORANDUM. Scientific and technical findings that are preliminary or of specialized interest, e.g., quick release reports, working papers, and bibliographies that contain minimal annotation. Does not contain extensive analysis.

- CONTRACTOR REPORT. Scientific and technical findings by NASA-sponsored contractors and grantees.

- CONFERENCE PUBLICATION. Collected papers from scientific and technical conferences, symposia, seminars, or other meetings sponsored or co-sponsored by NASA.

- SPECIAL PUBLICATION. Scientific, technical, or historical information from NASA programs, projects, and missions, often concerned with subjects having substantial public interest.

- TECHNICAL TRANSLATION. English-language translations of foreign scientific and technical material pertinent to NASA's mission.

Specialized services also include organizing and publishing research results, distributing specialized research announcements and feeds, providing information desk and personal search support, and enabling data exchange services.

For more information about the NASA STI program, see the following:

- Access the NASA STI program home page at http://www.sti.nasa.gov

.

NASA/TP–20260003940

Thermal Considerations for 2039 Opposition Class Nuclear Electric Propulsion/Chemical Propulsion Crewed Mars Mission

Tai Lily Valdés
Langley Research Center, Engineering Directorate, Structural and Thermal Systems Branch [Hampton, VA]

Will J. Grier, Amanda E. Stark
Langley Research Center, Engineering Directorate, Structural and Thermal Systems Branch [Hampton, VA]

National Aeronautics and

Space Administration

Langley Research Center
Hampton, Virginia

May 2026

Available from:

NASA STI Program / Mail Stop 050
NASA Langley Research Center
Hampton, VA 23681-2199

Table of Contents

Abstract....4
Acronyms and Nomenclature 5
1 Introduction 6
1.1 Mission Parameters 6
1.2 MARVL System of Interest 7
1.3 Radiator Wing Configuration 8
2 Objectives 8
3 Methods 9
3.1 Interaction of the Radiator Panel with the Space Thermal Environment 10
3.2 Thermal Modeling and Data Capture 13
3.3 Modeling to Capture Variations in Mission Trajectory 14
3.3.1 Definitions of Modeled Variables 14
3.3.2 Special Cases 16
3.4 Reduction of Cases to Capture the Thermal Environment 19
4 Results 20
5 Discussion....20
5.1 Selection of Ideal Panel Orientations 21
5.1.1 LEO 500 km and 1100 km....21
5.1.2 NRHO 21
5.1.3 Mars Orbits 22
5.1.4 Venus Flyby 22
5.1.5 Interplanetary Travel....22
5.2 Rapid Changes of Environmental Sink Temperature 22
5.2.1 Limitations in Identifying Rapid Change in Environmental Sink Temperature Due to Cylindrical Shadow Approximation 23
6 Conclusion and Future Work 23
Acknowledgements 23
References 24
Appendices 26
Appendix A. Thermal Environment Specification for Relevant Phases 26
A.1 Interplanetary Travel....27
A.2 Low Earth Orbit....27
A.3 Near-Rectilinear Halo Orbit....28
A.4 Lunar Distant High Earth Orbit 29
A.5 Mars Orbits 30
A.6 Venus Flyby 30
Appendix B. Comparison of Modeling Periapsis vs. Apoapsis on Sun-Side of Mars 31
Appendix C. Modeling Multiple Sequential Orbits....32

Appendix D. Summary of Selected Cases. 33
Appendix E. All Environmental Sink Temperature and Heat Rejection Capability Curves 35

Abstract

The high specific impulse (Isp) of Nuclear Electric Propulsion (NEP) technology offers the potential for advanced space mission capabilities. However, the five critical technology elements of NEP vehicles have yet to prove technical maturity levels for consideration into mission design. In response to the critical reviews by the NASA Engineering and Safety Center (NESC) [1] and the National Academies of Sciences, Engineering, and Medicine (NASEM) [2], NASA's Space Nuclear Propulsion (SNP) project created an NEP Technology Maturation Plan (TMP) for focused development of NEP technology [3]. The TMP called for a coordinated set of technology development efforts to meet this objective. The Modular Assembled Radiators for NEP VehicLes (MARVL) Early Career Initiative (ECI) project was initiated to develop a portion of the fifth Critical Technology Element (CTE) of the NEP vehicle: the Primary Heat Rejection Subsystem (PHRS). A target application of a 2039 human-rated Mars mission was outlined in the TMP. For the outlined mission, a NEP vehicle will experience several thermal environments which will impact the design and operation of the PHRS. To maintain radiator temperatures within the required effective temperature range, the effect of natural, induced, and NEP internally generated heat loads on the radiator panel must be well understood. Furthermore, this analysis is critical for analyzing the influence of various orientations and positions of the NEP vehicle relative to nearby celestial bodies throughout the mission. This study conducted a complete enveloping analysis of the thermal environments influencing the NEP vehicle throughout the mission. Thermal analysis was conducted for the radiator panels based on the defined mission environments. This thermal analysis concludes with the selection of ideal radiator orientations for the NEP vehicle, and the identification of worst case hot and cold environmental sink temperatures throughout the mission.

For the target application, the environmental sink temperature ranges from 30 K to 353 K when the reactor is powered OFF, and from 2.7 K to 243 K when it is powered ON. In interplanetary space, the minimum environmental sink temperature occurring when the reactor is powered OFF and the radiators are oriented "edge to Sun" is 2.7 K.

The environmental thermal models generated in this study will be used for future studies with the full vehicle system model. The environmental sink temperature curves generated will be used for future radiator and component analysis to predict transient performance in the space environment. The environmental sink temperature and heat rejection capability curves will inform the trade between commissioning orbits that are in consideration**.** The model may also serve as a useful tool as reference for future crewed space missions, missions involving radiators or temperature sensitive equipment, or other missions requiring analysis of natural orbital thermal environments.

Acronyms and Nomenclature

A_R = radiator surface area [m^2]
AU = astronomical unit
CTE = Critical Technology Element
ECI = Early Career Initiative
EPS = Electric Propulsion Subsystem
iSA = in-Space Assembly
I_{sp} = specific impulse [1/s]
IR = infrared
LDHEO = Lunar Distant High Earth Orbit
LEO = Low Earth Orbit
MARVL = Modular Assembled Radiators for NEP VehicLes
MW_e = Megawatts electric
MW_{th} = Megawatts thermal
NASEM = National Academies of Sciences, Engineering, and Medicine
NRHO = Near-Rectilinear Halo Orbit
NESC = NASA Engineering and Safety Center
NEP = Nuclear Electric Propulsion
OLR = outgoing longwave radiation
PCS = Power Conversion Subsystem
PHRS = Primary Heat Rejection Subsystem
PMAD = Power Management and Distribution Subsystem
q_A = total absorbed flux [W/m^2]
q_{IR} = incident IR flux [W/m^2]
q_s = incident solar flux [W/m^2]
Q = net thermal power emitted [W]
R_1 = fluid to heat pipe resistance [K/W]
R_2 = heat pipe to panel resistance [K/W]
R_c = heat rejection capability [%]
RAAN = right ascension of the ascending node
RXS = Nuclear Reactor and Coolant Subsystem
SACD = Systems Analysis and Concepts Directorate
SNP = Space Nuclear Propulsion
SOI = System of Interest
$T_{f_{avg}}$ = fluid increment average temperature [K]
$T_{f_{in}}$ = fluid increment inlet temperature [K]
$T_{f_{out}}$ = fluid increment outlet temperature [K]
T_{hp} = heat pipe temperature [K]
T_{inlet} = fluid loop inlet temperature [K]
T_{outlet} = fluid loop outlet temperature [K]
T_R = radiator temperature [K]
T_∞ = environmental sink temperature [K]
$T_{\infty_{tot}}$ = total environmental sink temperature [K]
$T_{\infty_{des}}$ = design sink temperature [K]
TD = Thermal Desktop
TMP = Technology Maturation Plan
TRL = Technology Readiness Level
VV = velocity vector
αps = power system specific mass [kg/kW$_e$]
Δv = change in velocity [m/s]
ε_{IR} = IR emissivity [unitless]
η = radiator effectiveness [unitless]
σ = Stefan-Boltzmann constant [W/m^{2}K^4]

1 Introduction

The integration of NEP technology into advanced mission designs and early human Mars missions reduces total transit time and enables deep space exploration and science. Previous crewed Mars mission studies were constrained to chemical propulsion systems, technologies with specific impulses (I_{sp}) below 450 seconds, which significantly limit performance on propulsively demanding, high-Δv missions[4]. Therefore, past missions were designed for conjunction class trajectory, defined by the positions of Mars and Earth on the same side of the Sun, and selected for the lower Δv requirements. However, a consequence of this design is the extended total mission duration [5].

In contrast, NEP technology significantly reduces the overall required propellant mass and increases Δv capabilities when compared to chemical propulsion systems, opening the possibility for mission designs of shorter durations. With high I_{sp} at over thousands of seconds [2, 3, 6], a hybrid nuclear electric propulsion (NEP)/chemical propulsion vehicle can enable mission designs advantageous for early crewed missions to Mars. One mission design enabled by this technology is the opposition class mission design, defined by positions of Mars and Earth on opposing sides of the Sun. This mission design is advantageous as high Δv maneuvers required for this trajectory result in shorter mission durations. For initial human Mars missions, shorter mission durations are ideal for reduced crew exposure to space hazards and risk, such as exposure to deep space radiation and duration in microgravity [5].

Since the late 1950s, several NEP programs have been pursued by NASA and the United States military including the Systems for Nuclear Auxiliary Power (U.S. Government initiative led by the Atomic Energy Commission, in collaboration with the U.S. Air Force and NASA), SP-100 Space Power Reactor (DOD, DOE, and NASA), Space Exploration Initiative (NASA), and Jupiter Icy Moons Orbiter/Prometheus (NASA) [2]. However, although NEP technology offers the potential for significant advances in mission capability, its critical technology elements (CTEs) have not yet achieved the technical maturity required to support credible mission architecture development. The five CTEs of the NEP vehicle include CTE1: Nuclear Reactor and Coolant Subsystem (RXS), CTE2: Power Conversion Subsystem (PCS), CTE3: Power Management and Distribution (PMAD), CTE4: Electric Propulsion Subsystem (EPS), and CTE5: Primary Heat Rejection Subsystem (PHRS) [3]. In a review of nuclear propulsion technical maturity by the NASA Engineering and Safety Center (NESC) [1], the key NEP technologies were identified at or below Technology Readiness Level (TRL) 4, with even lower maturity at the system and subsystem levels. The vehicle assessed was a hybrid NEP/chemical propulsion vehicle. The National Academies of Sciences, Engineering, and Medicine (NASEM) subsequently conducted a review [2] of the NEP/chemical propulsion vehicle and concluded that the primary factor limiting NEP system advancement is the lack of coordinated development and research focused on demonstrating megawatts electric (MW_e)-class hardware at TRL 5.

In response to the critical reviews by the NESC [1] and NASEM [2], NASA's Space Nuclear Propulsion (SNP) project created an NEP Technology Maturation Plan (TMP) for focused development of NEP technology [3]. The mission plan developed in the TMP led to the creation of the Modular Assembled Radiators for NEP VehicLes (MARVL) Early Career Initiative (ECI) project, to develop a portion of the CTE5 of the NEP vehicle: the Primary Heat Rejection Subsystem (PHRS). The project is a Langley Research Center led cross-agency team including personnel from Langley Research Center, Glenn Research Center, Kennedy Space Center, Marshall Space Flight Center, and Johnson Space Center.

1.1 Mission Parameters

To capture the wide variety of possible mission phases and environments for crewed missions to Mars, a target application was outlined in the TMP for NEP technology development. This target application from a thermal perspective is not a singular mission, but rather an enveloping opposition-class mission which encompasses the possible trajectories and orbits of multiple previous mission studies. The term opposition is defined by Mars' location relative to Earth and determines the duration of various phases for the mission. The trajectory for the opposition class mission is shown below in Figure 1.

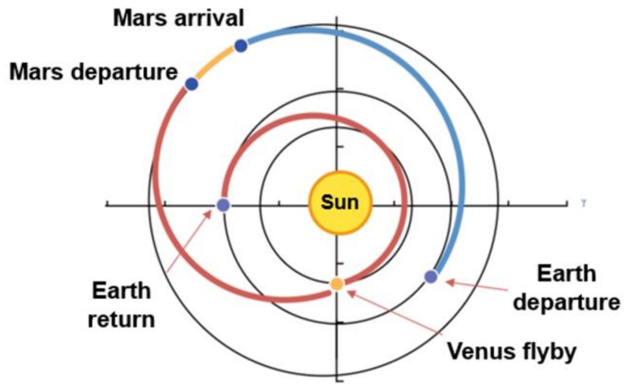

Figure 1. Mission locations of the opposition class trajectory [5]**.**

The target application has a crew departure date of 2039 with a total mission duration of around 3 years [3, 7]. The NEP system will be used for cruise phases, and the chemical stage will be used to enter and exit gravity wells. The possible mission locations include Low Earth Orbit (LEO), Near-Rectilinear Halo Orbit (NRHO), Lunar Distant High Earth Orbit (LDHEO), Mars orbit, a Venus flyby, and interplanetary space. A relevant environment is the specific subset of the operational environment required to demonstrate critical "at risk" aspects of final product performance [8]. The relevant environments for this mission include thermal, vacuum, micrometeoroid and orbital debris, radiation, launch loads, in-space loads, and microgravity. The focus of this study is on thermal environments for the mission.

1.2 MARVL System of Interest

The overall power level of the PCS is estimated at 2-4 MW_e [3]. A Brayton cycle is used to convert heat from the reactor into electric power. As a part of this cycle the PCS generates waste heat to be rejected which for a 2 MW_e vehicle is estimated to produce a power output of 4 megawatts thermal (MW_{th}) [3]. The amount of thermal energy that will be generated over time is too significant to be repurposed by the vehicle and must be rejected into space. The three key functions of the PHRS are to 1) accept waste heat generated in the PCS, 2) transport waste heat, and 3) radiatively reject waste heat to space. The MARVL system of interest (SOI) is a portion of the PHRS. In terms of thermal components, the SOI includes the fluid loops, fluid interfaces between the fluid loops and radiator panels, and radiator panels. The MARVL SOI within the PHRS is illustrated below in Figure 2.

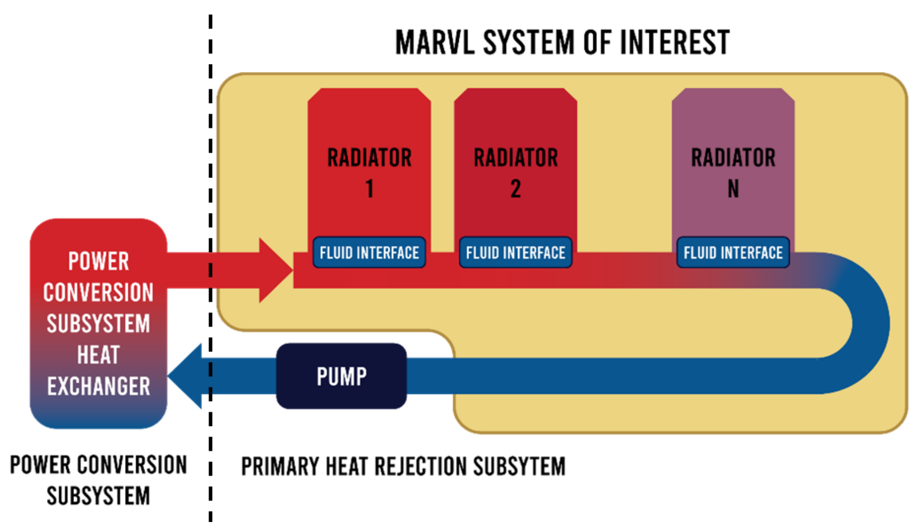

Figure 2. **The MARVL System of Interest (SOI) is found within the PHRS and consists of fluid loops, radiators, and fluid interfaces.**

Due to the large amount of waste heat generated by the PCS, the PHRS is the largest and most massive of the five CTEs. The PHRS constitutes 40-60% of the total NEP dry mass, with an estimated surface area >3,000 m^2 [9]. A key metric for the performance and feasibility of the NEP system is the power system specific mass, or α_{ps} [kg/kW$_e$] [10]. The PHRS is the largest contributor, estimated at around 50% of the total system α_{ps} [11]. Reduction in PHRS mass is key in terms of optimizing vehicle performance, with a threshold for minimum success of 8 kg/kWe and a goal for maximum success of 3.5 kg/kWe.

1.3 Radiator Wing Configuration

The selected wing configuration for the PHRS is a bi-wing configuration (Figure 3a). This wing design is advantageous as it can be flown edge-on to the Sun or to nearby celestial bodies which reduces incident heat loads. Additionally, wing-to-wing view factors are minimized. Therefore, the heat rejection capability of the bi-wing configuration is more effective than that of the quad-wing design (Figure 3b). The TMP integrates in-Space Assembly (iSA) into the PHRS design, which allows for expanded possibilities for radiator configurations. Greater effectiveness of the bi-wing panels allows for a reduction in total panel surface area, which leads to about a 20-40% dry mass reduction [9] when compared to quad-wing designs.

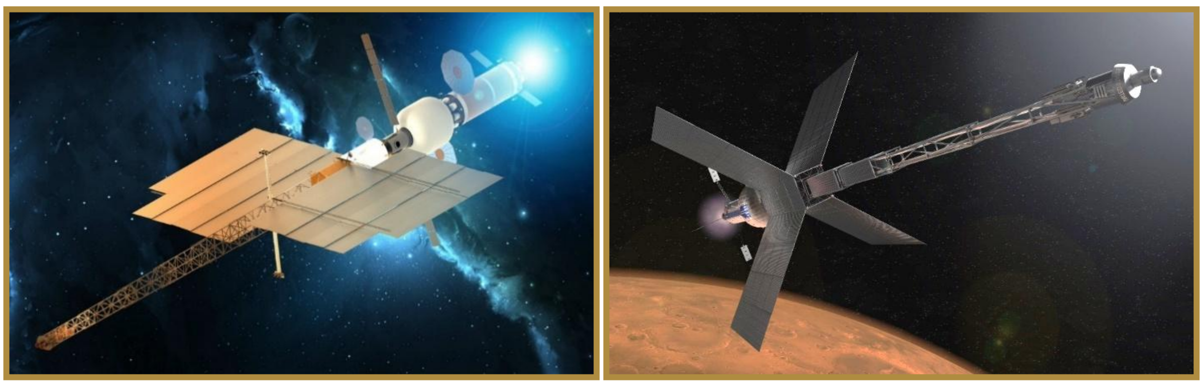

(a) **(b)**

Figure 3. Representative conceptual illustration of the (a) bi-wing and (b) quad-wing panel configurations. The MARVL project focuses on the development of the bi-wing configuration and the design of a modularized in-space assembled system for the PHRS.

2 Objectives

The objectives of the study can be summarized into four parts: 1) envelope the wide variety of mission phases to define the worst case hot and cold environments, 2) understand the effect of panel orientation on environmental sink temperature and heat rejection capability, 3) select ideal panel orientations to align with radiator temperature and heat rejection capability constraints, and 4) identify the absolute extrema of environmental heat sink temperatures across the mission.

This study identifies the most extreme thermal environments influencing the NEP vehicle throughout all phases of a 2039 crewed opposition class Mars mission. The thermal environment describes the effective temperature of the surrounding environment that acts as a thermal sink for radiative heat transfer from a surface. The environmental sink temperature represents a complex radiation environment as a single equivalent temperature value [12]. Worst case hot and cold effective environmental temperature values are identified for the mission. Environmental sink temperature and heat rejection capability are influenced by radiator orientation and position of the NEP vehicle, due to view factors of the radiator panels to nearby celestial bodies. This analysis varies the orientation and position of the radiator panel to select ideal panel orientations across the range of mission phases and locations.

Mission phases for consideration include LEO, NRHO, LDHEO, Mars orbits, Venus flyby, and interplanetary space. The space environment thermal inputs include direct solar radiation, solar radiation reflected from nearby planets also known as albedo, and planetary infrared (IR) also known as outgoing longwave radiation (OLR). Additional considerations include selection of planetary albedo and IR worst-case values, wavelength band sensitivity of the radiator surface finish, capturing maximum and minimum direct solar radiation values for each mission location that account for variation in specific spacecraft paths, considerations for eclipse cases, and beta angles. Surveys were conducted from various resources and NASA documentation [13, 14, 15, 16, 17, 18, 19] to identify the hot and cold values of nearby heating sources in the space environment and these values are detailed in Appendix A.

The relationship between the heat rejection of the radiator panels, the average radiator temperature, and environmental sink temperature is illustrated in Figure 4. Like the mission analyzed in the study, the radiator temperature is held at a constant effective temperature of 400 K [9]. At 0 K environmental sink temperature, the heat rejection capability is at the maximum, 100%. As the environmental sink temperature reaches the radiator temperature, 400 K, the heat rejection capability reaches 0%. The calculations behind this analysis are defined by Equations 1, 6, and 7 in Section 3.1.

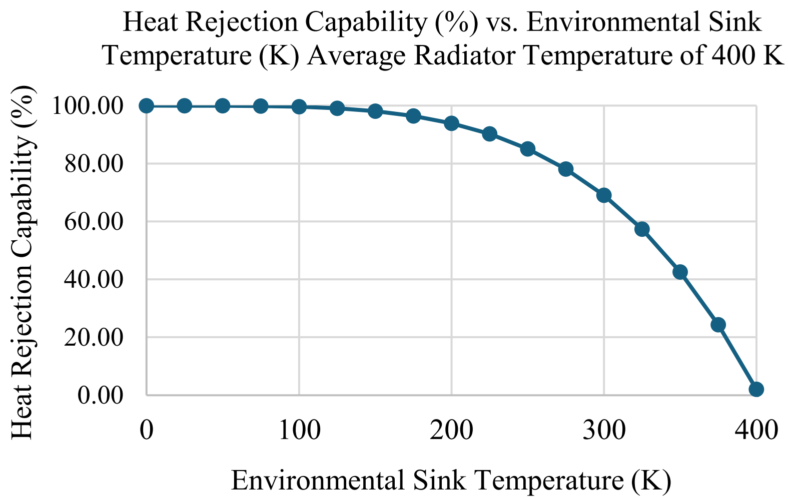

Figure 4. Relationship between three key thermal factors for the radiators: heat rejection capability, environmental sink temperature, and average radiator temperature.

Reactor power levels vary from powered OFF to fully powered ON in the MARVL target application, dependent on the mission phase and reactor power requirements. In this study, the radiator temperature is maintained at a constant average temperature of 400 K due to thermal performance limits of the water-based heat pipes. There are two variables that can be manipulated to keep this constant radiator temperature. First, the environmental sink temperature is dependent on NEP vehicle location but can be altered by changing panel orientation. Second, the internally generated waste heat load of the NEP system can be altered by throttling the reactor and PCS power levels.

The objective of this study is to analyze the effect of panel orientation on environmental sink temperature and heat rejection capability, and to identify viable panel orientations. The environmental sink temperature varies significantly with mission location and panel orientation. Altering the panel orientation for a given mission location affects the view factor between the panel and nearby environmental heating sources, which alters the derived environmental sink temperature without compromising mission trajectory. Once ideal panel orientations are selected, the extrema of thermal environments throughout the mission will be captured.

3 Methods

This study captures the environmental heating source extrema at each mission phase. Specifically, the hot and cold cases for direct solar, albedo, and OLR at LEO, NRHO, LDHEO, Mars orbits, Venus flyby, and interplanetary space. The values, provided in the summary tables in Appendix A, were used as inputs to the Thermal Desktop (TD) model. The Methods section is divided into four parts: 1) interaction of the panel with the space thermal environment, 2) Thermal Desktop model setup, 3) modeling to capture variations in mission trajectory, and 4) selection of ideal panel orientations and beta angles to reduce cases.

3.1 Interaction of the Radiator Panel with the Space Thermal Environment

The net thermal power emitted by the radiator surfaces is described in Equation 1 [12, 13],

$$Q = A_R \varepsilon_{IR} \sigma \eta (T_R^4 - T_{\infty_{tot}}^4) \tag{1}$$

where Q is the net thermal power emitted [W], A_R is the radiator surface area [m^2], ε_{IR} is the IR emissivity [unitless], σ is the Stefan-Boltzmann constant [W/m^{2}K^4], η is the radiator effectiveness [unitless], T_R is the radiator temperature [K], and $T_{\infty_{tot}}$ is the total environmental sink temperature [K]. The net thermal power emitted is equal to the thermal emission rate minus the thermal absorption rate from the environment.

Radiator panel net heating is comprised of several sources. T_R is driven by the waste heat generated by the PCS and carried in the thermal trunkline to the PHRS. $T_{\infty_{tot}}$ depends on various sources including from the space environment, IR emitted from the NEP vehicle, and solar radiation reflected off the NEP vehicle. The effect of IR emitted from the vehicle and reflected solar radiation from the vehicle are dependent on vehicle geometry. These effects are expected to be small compared to the rest of the sources and will be neglected in this study but will be analyzed in future studies. Therefore, for this study $T_{\infty_{tot}}$ is calculated only from view factors of the panel to heating sources in the space environment.

The radiator array thermal network, shown in Figure 5, consists of the fluid loop inlet temperature T_{inlet} [K], fluid loop outlet temperature T_{outlet} [K], fluid increment inlet temperature $T_{f_{in}}$ [K], fluid increment outlet temperature $T_{f_{out}}$ [K], fluid increment average temperature $T_{f_{avg}}$ [K], fluid to heat pipe resistance R_1 [K/W], heat pipe to panel resistance R_2 [K/W], heat pipe temperature T_{hp} [K], and total environmental sink temperature T_∞.

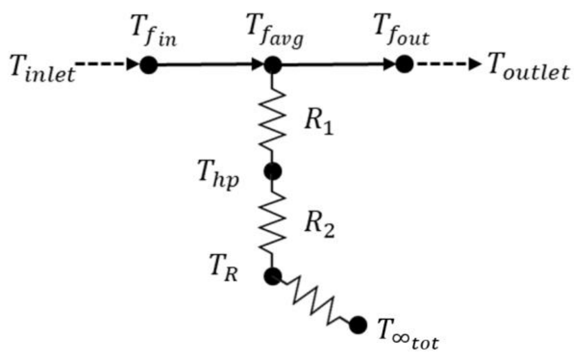

Figure 5. Radiator array thermal network.

In this study, T_R is held constant at 400 K. This represents the area-weighted average surface temperature of the radiator considering thermal resistances and associated temperature drops along the radiator array length. The T_R variable is determined via the effective individual radiator temperatures, calculated from a thermal network with an iterative numerical method. Major variables in the analysis include working fluid inlet and outlet temperatures, working fluid mass flow rate, radiator increment area A_i [m^2], working fluid specific heat capacity, heat pipe to panel thermal resistance, heat pipe spacing, and thermal conductivity of radiator panel face sheet [W/K]. The radiator array operates at progressively cooler temperatures along its length, and the effective temperature accounts for this variation.

The following relationships for $T_{f_{avg}}$, T_{hp}, Q_{rej}, and T_R are utilized in the iterative numerical analysis.

$$Q_{rej} = A_i \varepsilon_{IR} \sigma \eta (T_R^4 - T_{\infty_{tot}}^4) \tag{2}$$

$$T_{f_{avg}} = \frac{T_{f_{out}} - T_{f_{in}}}{2} \tag{3}$$

$$T_{hp} = T_{f_{avg}} - Q_{rej}R_1 \quad (4)$$

$$T_R = T_{hp} - Q_{rej}R_2 \quad (5)$$

The assumptions for all other variables are described in the remainder of this section.

The fluid to heat pipe resistance R_2 is the inverse of the fluid to heat pipe conductance (assumed to be 1000 W/K), so $R_1 = 1/1000$ K/W, and the fluid to heat pipe conductance R_2 is the inverse of the heat pipe to panel conductance (assumed to be 1000 W/K), so $R_2 = 1/1000$ K/W.

The working fluid inlet temperature T_{inlet} of 550 K and outlet temperature T_{outlet} of 330 K were identified via numerical methods of the energy balance for the MARVL thermal network including fluid loop, heat pipe, and radiator design variables, with interfaces to the NEP PCS considered. When exceeding the outlet temperature limit, there is significant NEP system mass increase, as the PCS cycle efficiency decreases thereby increasing the waste heat load [9]. Furthermore, regarding the inlet temperature limit, the heat pipes are designed with water as the working fluid due to the higher TRL level of this design compared to other options (e.g., cesium or halide based working fluids). With water as the working fluid, higher temperatures can cause various issues. First, higher temperatures can dry out the heat pipes, preventing heat transfer and causing risk of damage [9], and second, the boiling limit must not be exceeded as this may cause the fluid to evaporate and increase internal pressure which leads to mass increases due to increased heat pipe wall thickness. The returning fluid will travel to the PCS heat exchanger and is limited to 330 K, determined based on the results of an integrated NEP parametric analysis that optimizes system mass and performance.

The radiator effectiveness is dependent on heat pipe spacing and fin geometry [13]. In this study, a conservative radiator panel effectiveness of $\eta = 0.85$ is assumed for this preliminary analysis of the MARVL radiator system.

Next, the heat rejection capability R_c of the radiator panels can be calculated as a percentage using Equation 1. The capability for heat rejection is defined as emitted heat at a given environmental sink temperature compared to heat rejection achieved at the design sink temperature. The percent heat rejection capability is:

$$R_c = \left(\frac{A_R \varepsilon_{IR} \sigma \eta \left(T_R^4 - T_{\infty_{tot}}^4\right)}{A_R \varepsilon_{IR} \sigma \eta \left(T_R^4 - T_{\infty_{des}}^4\right)}\right) * 100 \quad (6)$$

where $T_{\infty_{des}}$ is the design sink temperature which is the baseline capability of the vehicle. For this study, the design sink temperature is at 0 K, so the maximum heat rejection capability is achieved when no external sources of heat load are incident on the radiator panels. When $T_{\infty_{des}} = 0$ K, the calculation can be simplified as shown in Equation 7. The relationship between Q, T_R, and R_c is also discussed in Section 2 and illustrated in Figure 4.

$$R_c = \frac{\left(T_R^4 - T_{\infty_{tot}}^4\right)}{T_R^4} * 100 \quad (7)$$

Since $T_{\infty_{des}} = 0$ K throughout this study, the total environmental sink temperature $T_{\infty_{tot}}$ will instead be referred to as T_∞ for simplicity.

Space thermal environment interactions with the radiator panel are illustrated in Figure 6. As depicted, the two bands of thermal radiation interacting with this panel are sunlight (solar band radiation) and IR radiation. The radiator panel receives direct solar radiation, solar radiation reflected from nearby planets also known as albedo, and IR radiation emitted from nearby planets. The thermal radiation that reaches the radiator is either reflected off the panel or absorbed. The combined energy from both thermal radiation and heat transfer from the fluid loops that is absorbed by the panel causes it to heat up, which could increase radiator temperature past the 550 K limit of the water-based heat pipes if the heat transfer from the fluid loop is not decreased. The absorbed heat energy is then rejected from the radiator surface by IR radiation. The induced thermal environment caused by emitted and reflected heat fluxes from the NEP vehicle incident upon the panels is not included in this study.

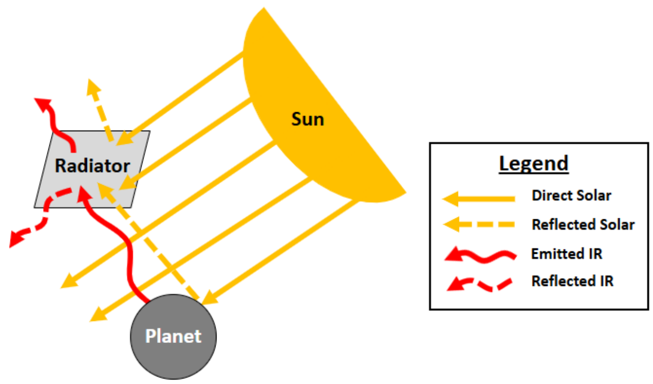

Figure 6. Illustration of the interaction between a radiator panel and the space thermal environment.

The panel optical properties affect how the thermal radiation incident on the panel is either absorbed or reflected. The fraction of solar radiation absorbed by the panel, and the effectiveness of a material to emit IR radiation compared to an ideal blackbody at a given temperature, is described by the material's solar absorptivity (α_s) and IR emissivity (ε_{IR}) respectively [13].

Requirements for the optical properties of the MARVL radiator surface will depend on radiator surface material, operating temperature range, and mission flight profile (e.g., property degradation over mission life) [3]. The current material in consideration for the radiator surfaces is a carbon-based material, specifically graphite composites with thermally conductive fibers [20]. Typical carbon-based materials have an emissivity between 0.85 and 0.9, and in the NEP TMP, 0.85 is identified as the minimum threshold for end-of-life IR emissivity [3]. This study assumes a conservative estimate of 0.85. This value is subject to change with future material tests. The value for α_s is also subject to change and is currently assumed at 0.7. The absorptivity of the carbon-based composite material is higher than the value mentioned previously for typical radiators because currently, no low solar absorptivity coatings exist rated for >550 K applications. The coatings are limited by the performance of the adhesive or binder when exposed to higher temperatures. Orientation of the radiator panels in an edge on to the Sun configuration is an avenue to mitigate greater than desired absorbed solar flux caused by high solar absorptivity materials. The effect of panel orientations will be analyzed in depth in this study.

The summary of current assumptions for optical properties for the MARVL radiators is shown in Table 1. With material selection and further analysis, optical property values are subject to change later in the radiator design process. The optical property values are parameterized in this study, allowing for future changes to these assumptions. This process is further described in Section 3.2.

Table 1. Conservative Assumptions for MARVL Radiator Optical Properties.

Optical Property	Conservative Assumption for MARVL Radiators
α_s	0.7
ε_{IR}	0.85

3.2 Thermal Modeling and Data Capture

With the environmental heating sources defined in Appendix A, the next step was capturing the interaction between the radiator panels and the space thermal environment. The commercial thermal analysis software C&R Technologies Thermal Desktop (TD) version 6.3 was used to model orbital cases and trajectories to then apply and record the heating source values. This model was also used to measure the effect of altering the view factors between the panel and nearby celestial bodies.

The objective of the model was to measure the space thermal environment depending only on location of the panel and view factor of the panel to heating sources. This model uses a representative 1 m x 1 m panel with 0 m thickness, with arithmetic nodes set to record instantaneous flux values. The justification is as follows:

1. The 1 m x 1 m surface dimensions of the panel are reasonable as only specific incident fluxes (W/m^2) are measured. Additionally, the change in location across the MARVL radiator wings (one side ~1200 m^2) is insignificant compared to the position in space relative to the Sun and other celestial bodies.
2. The model has a 0 m thickness to isolate the effect of view factor from the flat face to the heating sources. The MARVL radiator panels are relatively thin, on the order of less than a few inches in thickness, thus there is a negligible effect on view factor to heating source.
3. The use of arithmetic nodes is a reasonable representation of the panel as the assumptions are that the radiator will have a low thermal time constant (10s of seconds to minutes) [21]. Additionally, the temperature of the radiator surface in the Thermal Desktop model does not affect results as radiator-to-radiator view factor is not modeled. This is a reasonable representation of the bi-wing radiator arrays which will be relatively flat with some deflection errors.

The IR emissivity and solar absorptivity values were both set to one within the TD model to represent the panel as a black-body surface. Doing this enables the TD model to capture only the incident fluxes (solar and IR). The application of radiator surface optical properties was then parameterized as a variable in the data collection and post-processing step to calculate total absorbed flux. This method is applicable for this study because the panel was modeled as a single flat surface, thus there are no surface-to-surface view factors or reflections. One advantage of this approach is the optical property assumptions can be changed later as needed, or for future analysis of different materials in the same space environment, all without re-running the TD models.

> **Note:** if solar absorptivity assumptions lower significantly, then the heating source input values used in the TD models must be updated to reflect material sensitivity to IR only. More information on material sensitivity and the selection of heating source inputs can be found in Appendix A.2.

Outputs generated include hot and cold cases for time-varying (single orbit) incident flux values for each space location, panel orientation, and solar beta angle variation. Next, every solar and IR incident flux value calculated in TD was recorded in Microsoft Excel. The assumptions for the MARVL radiator optical properties were applied in this step. Equation 8 shows the calculation for total absorbed flux [22, p. 38].

$$q_A = (\alpha_s * q_s) + (\varepsilon_{IR} * q_{IR}) \tag{8}$$

Where q_A is the total absorbed flux [W/m^2], q_s is incident solar flux [W/m^2], and q_{IR} is incident IR flux [W/m^2]. In this step, the optical properties $\alpha_s = 0.7$ and $\varepsilon_{IR} = 0.85$ were specified in Excel. This equation was applied to all output incident flux values that were calculated in TD. Next, using the absorbed flux values, environmental sink temperatures were calculated using Equation 9 [22, p. 38].

$$T_{\infty_{tot}} = \left(\frac{q_A}{\sigma * \varepsilon_{IR}}\right)^{\frac{1}{4}} \tag{9}$$

This calculation was solved for every time step calculated in TD, providing insight into the $T_{\infty_{tot}}$ fluctuations throughout the vehicle's orbital paths. Finally, the radiator panel temperature was also parameterized as a variable in Excel. The $T_{\infty_{tot}}$ values and assumed radiator temperature T_R are used to solve for R_c values using Equation 7.

3.3 Modeling to Capture Variations in Mission Trajectory

This study focuses on LEO, NRHO, Mars orbits, and a Venus flyby, and excludes analysis of LDHEO. LDHEO was excluded due to modeling complexity, but orbital parameters and thermal values for LDHEO heating source inputs are included in Appendix A.4. Considered in the model are orbit altitudes, orbit eccentricities, trajectories, beta angles, and hot/cold cases; this results in a total of 328 different cases ran in this study. A breakdown of the 328 cases is provided in Figure 7, and the modeling parameters selected for modeling are also described in this section.

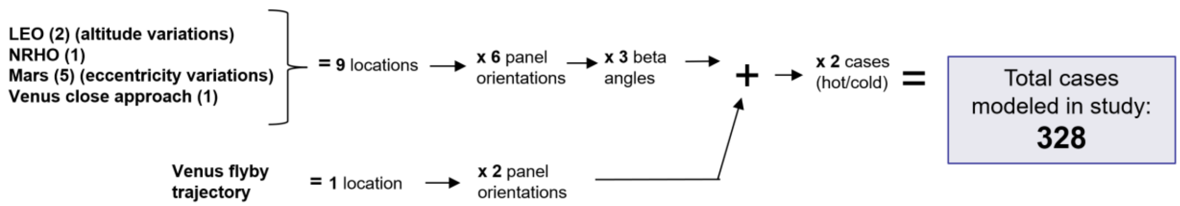

Figure 7. Summary of 328 total cases modeled in Thermal Desktop.

3.3.1 Definitions of Modeled Variables

This section includes detailed information regarding modeled variables described in Figure 7 that make up the 328 cases ran in the study.

3.3.1.1 Locations

The general in-space mission locations of LEO, NRHO, Mars orbits, and Venus flyby, have been expanded into 10 specific locations for analysis. The expansion is shown in Table 2.

Table 2. Expansion of general in-space mission locations into 10 modeled orbits and trajectories.

Mission Location	Orbit/Trajectory Specifications	Number of Orbital Configurations Modeled
LEO	500 km orbit, 1100 km orbit	2
NRHO	9:2 Lunar Synodic Resonant, Southern L2 Lagrangian Point	1
Mars orbits	250x7660 km (<1-Sol), 1-Sol, 2-Sol, 5-Sol, 10-Sol	5
Venus flyby	Sample Venus flyby trajectory, finite altitudes model	2

The NASA Gateway 9:2 Lunar Synodic Resonant specification was selected for the MARVL NRHO, due to its analysis for the planned Gateway Space Station. Specification of this orbit considers Lagrange (or libration) points, with L1 and L2 associated with halo orbits and closest to the moon. In these Lagrange points, there can also be NRHOs specified as either in the northern or southern family. Of the specifications, the L2 southern family NRHO was selected for better stability and visibility to the lunar far side for communications, as compared to L1 [23]. Furthermore, Lunar Synodic Resonant is a phasing specification which was selected to avoid eclipses by the Earth. This phasing avoids Earth shadow from January 2020 to February 2035, with only two partial eclipses occurring in 2034 and 2035. Finally, the 9:2 specification means the orbit completes on average, 9 revolutions for every 2 lunar months. This specification allows for easier surface access for the Gateway design, with a lower altitude perilune [23]. More detailed information about the orbital parameters for NRHO and for every in-space mission phase is provided in Appendix A.

Figure 8 depicts each of the models in TD. The orbital plane of the vehicle is represented by the yellow ellipse, and the shadow of the planetary body is represented by the purple cylinder.

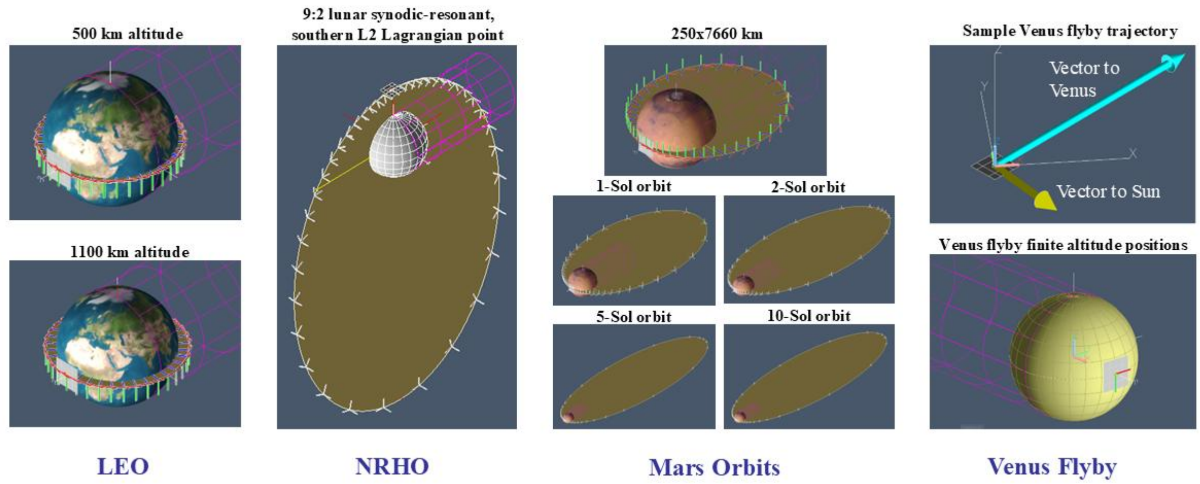

Figure 8. The ten total orbits and trajectories modeled in Thermal Desktop.

3.3.1.2 Panel Orientations

For LEO, NRHO, LDHEO, and Mars orbits, there are six panel orientations that are modeled in the TD model. The panel is oriented relative to the velocity vector (VV) of the NEP vehicle trajectory, and to the central body. The panel orientations include: "face to planet (edge to VV)", "edge to planet (edge to VV)", "edge to planet (face to VV)", "face to sun", "edge to Sun (horizontal)", and "edge to Sun (vertical)". For NRHO substitute "Moon" for "planet". Each panel orientation is shown in Figure 9, depicted for the ±52° beta angle LEO, at 1100 km altitude case.

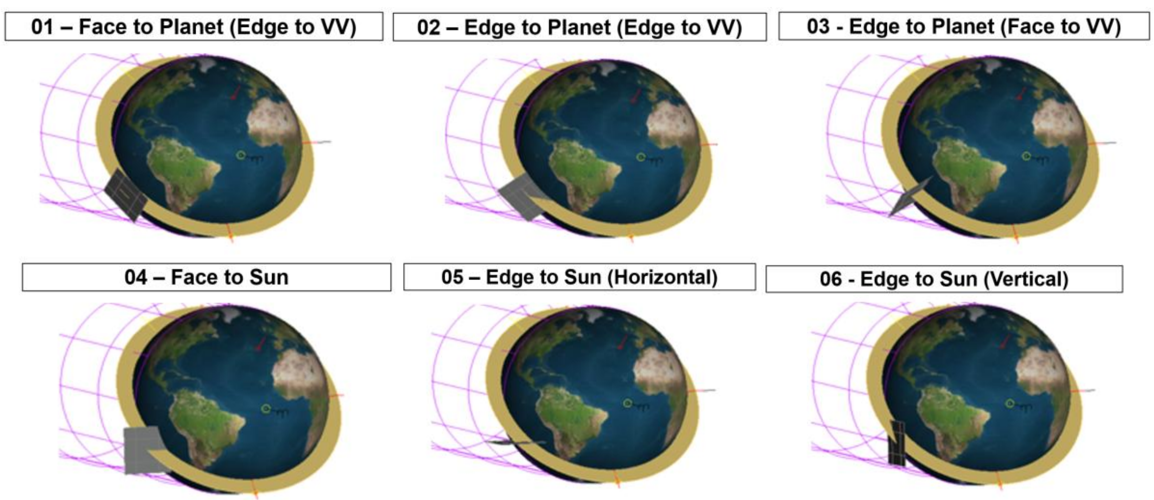

Figure 9. The six panel orientations modeled in TD for the LEO 500 km orbit. The same panel orientations were modeled for LEO, NRHO, LDHEO, and Mars orbits.

3.3.1.3 Beta Angles

The model includes cases for the range of possible solar beta angles. The solar beta angle represents the angle between the solar vector and the orbital plane. Specifying beta angles is important when modeling the thermal environment as altering the beta angle affects the incident environmental heating, the view factor of the panel to the Sun and nearby celestial bodies, and time spent in shadow. The beta angle sweep was modeled to capture the extreme thermal environments across the range of possible beta angles. The beta angle is described in Equation 10 [24], and is limited by:

$$\beta = \pm(\epsilon + |i|) \quad (10)$$

Over the range of

$$-90° < \beta < +90°$$

where β is the beta angle [degrees], ϵ is the obliquity of the ecliptic (or planetary tilt) [degrees], and i is the orbital inclination (the angle between orbital plane and equatorial plane) [degrees]. Whether the Sun is north or south of the orbital plane determines if the beta angle is considered positive or negative, respectively. The beta angle ranges between ± 90° for all orbits, except for LEO, which has a range between ± 51° based on a defined orbital inclination of 28.5° [25] (Appendix A).

The motivation for representing various beta angles in the orbital modeling is twofold: first, since not all phases in the target mission have an inclination angle defined (Appendix A), the model includes a sweep of possibilities for the target mission. Second, even for a fixed orbital inclination angle, the beta angle will change over time due to right-ascension of the ascending node (RAAN) shifts. Therefore, the model includes three beta angle increments for each case to bound the beta angle sweep, ranging from 0° to the maximum beta angle. An example of the three beta angles modeled for <1-Sol Mars orbit is shown in Figure 10.

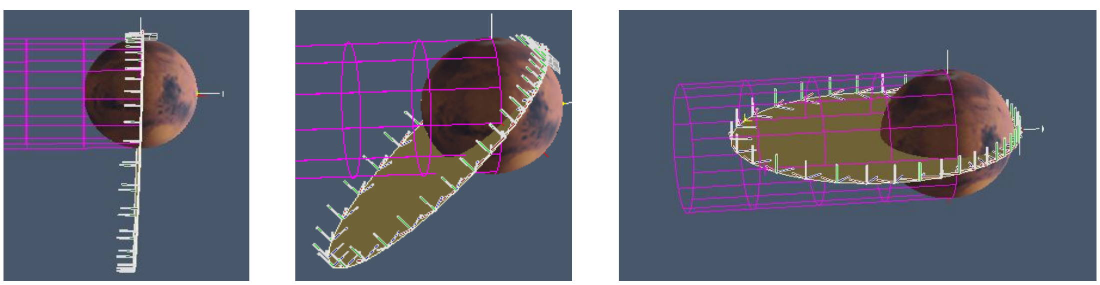

(a) (b) (c)

Figure 10. Variations modeled for <1-Sol Mars orbit represent (a) ±90° (b) ±45° (c) ±0° beta angles.

3.3.1.4 Hot and Cold Cases

All combinations of mission locations, panel orientations, and beta angles were modeled for both hot and cold-biased heat source input values, including direct solar, albedo, and IR radiation. In the TD model, the hot case uses heating source inputs with the hot case extreme values, and the cold case uses heating source inputs with the cold case extreme values (Appendix A). The worst-case hot and cold thermal environmental inputs represent bounding cases for the mission based on variation in planetary locations due to time of year, and position of the vehicle relative to the planet. Due to more observational data on IR and albedo values throughout the year for Earth, values for heating source inputs for Earth orbits also depend on material sensitivity to albedo and IR, thermal time constants for the radiator material, orbit inclination, and orbit beta angle albedo correction factors.

3.3.2 Special Cases

The cases described in Figure 7Table 7 describe much of the target mission trajectory, but there are additional considerations in the model to fully bound the thermal environments. This section describes the additional modeling considerations.

3.3.2.1 Vehicle Passage Through Shadow of Celestial Bodies

The coldest environment in an orbit occurs when the vehicle passes through the shadow of a celestial body. This section describes the various eclipse modeling considerations.

3.3.2.1.1 Cylindrical Shadow Approximation

The shadow behind celestial bodies is not naturally a cylindrical shape. Rather, it is a conical shape and has two regions within the shadow. The umbra is the region of the shadow where radiation intensity is close to zero. The penumbra includes both the umbral region and the region around the umbra of partial sunlight. For this study, all orbits have shadows modeled using a cylindrical shadow approximation (Figure 11).

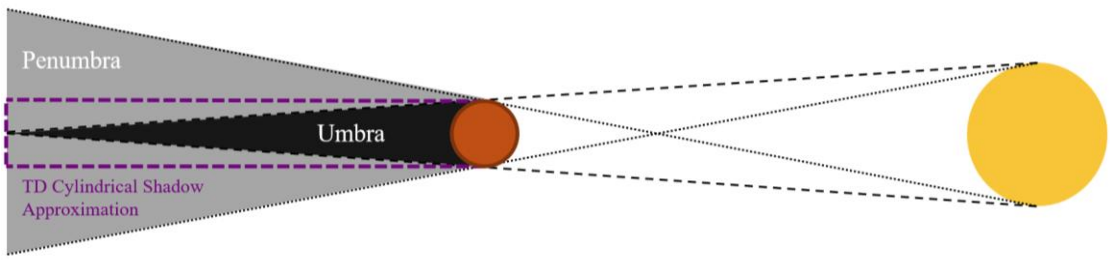

Figure 11. Comparison of penumbra and umbra regions of conical shadow with cylindrical shadow approximation that was modeled in Thermal Desktop.

The modeling of penumbra and umbra regions is more complex and is reserved for future work where the objective is to study components with higher thermal time constants and the performance of components throughout the orbit is more significant. The cylindrical shadow approximation will not affect the extrema of T_∞ and R_c values identified in the study but will overestimate the rate of change in these values at shadow crossings. Therefore, even with this approximation the results for orbital cases will be conservative and represent the worst case, because the shadow crossing will be more gradual than presented.

Earth orbits, NRHO, and less elliptical Mars orbits will not be significantly impacted by the cylindrical shadow approximation. However, with more elliptical orbits the panel will see more gradual entry into shadow as the duration in penumbra region would be longer when farther away from Mars. Thus, modeling the penumbra and umbra shadow regions is an area of future work for studies which require more accurate models of the thermal conditions for shadow entry and exit. As the objective of the study is to capture the extrema of thermal environments, the cylindrical shadow approximation is sufficient for the purpose of this study.

3.3.2.1.2 Measurement Positions for Capturing Eclipse Shadow Entry and Exit

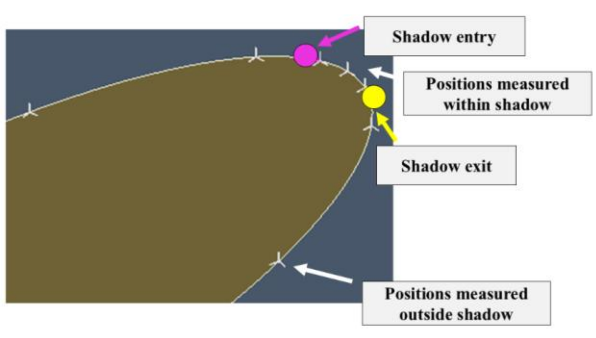

Figure 12. The 5-Sol Mars orbit for 0° beta angle around the point of apoapsis. Position intervals are adjusted for more eccentric orbits to include shadow entry and exit.

As the cylindrical shadow approximation is used for modeling the eclipse cases, the position of measurements is adjusted to more accurately capture the shadow entry and exit in the model. For the 500 km and 1100 km altitude LEO, NRHO, and <1-Sol and 1-Sol Mars orbits, the orbit was subdivided into 39 equal angular increments in TD, and the panel positions within the eclipses were captured. The analysis positions can be seen in Figure 10 for the <1-Sol Mars orbit, represented as white orientation markers around the orbital plane. In contrast, for the highly eccentric Mars 2-Sol, 5-Sol, and 10-Sol orbits, there were positions that skipped over the shadow during the 0° beta angle orbit. Therefore, the analysis increments were adjusted to read just before and within the shadowed region to improve precision and most accurately represent the coldest cases. This is shown in Figure 12.

3.3.2.1.3 Modeling Eclipse Cases for NRHO

The 9:2 Lunar Synodic Resonant NRHO is based on the Gateway orbit parameters [14] and introduces two additional eclipse considerations (Appendix A.3.1). The first consideration is passage through the Moon's shadow. Passage through the Moon's shadow is always less than 76.1 minutes for the NRHO, and the range of eclipse durations are captured in Table 8. The maximum passage duration through the penumbra (partial shadow) is 76.1 minutes, and the maximum passage through the umbra (total shadow) is 73.2 minutes. In this study, the NRHO is modeled using a Keplerian approximation of the orbit (Appendix A.3) with a cylindrical shadow approximation which captures an eclipse duration of 74.24 minutes.

The second eclipse consideration is passage through Earth's shadow. This eclipse can extend longer than 90-minutes without mindful NRHO trajectory design. The reasons for the longer eclipse duration is as follows: 1) Earth's shadow is larger than the Moon's shadow when viewed by the spacecraft in NRHO, and 2) spacecraft passage through Earth's shadow is typically of longer duration due to slower orbital velocity near apolune where Earth's shadow usually occurs along the NRHO [14]. The Lunar Synodic Resonant NRHO mostly avoids eclipses by Earth shadow from January 2020 to February 2035, though two partial eclipses occur during 2034 and 2035 [14, 23]. Therefore, additional planning may be considered to avoid Earth shadow for the 2039 mission.

3.3.2.2 Orientation of Eccentric Orbits

The orientation of eccentric orbits within the model is a consideration for the NRHO and Mars orbits. By identifying the orbit orientation that represents the worst-case conditions, the number of cases can be reduced. Figure 13 illustrates the 0° beta angle for the 1-Sol Mars orbit, where the periapsis is on the Sun side or the apoapsis is on the Sun side. Results and analysis from modeling the two cases are described in Appendix B. Resulting from this analysis, periapsis on the sun-side of the central body represents worst-case hot and cold environmental sink temperatures. Therefore, eccentric orbits for NRHO and Mars orbits follow this specification.

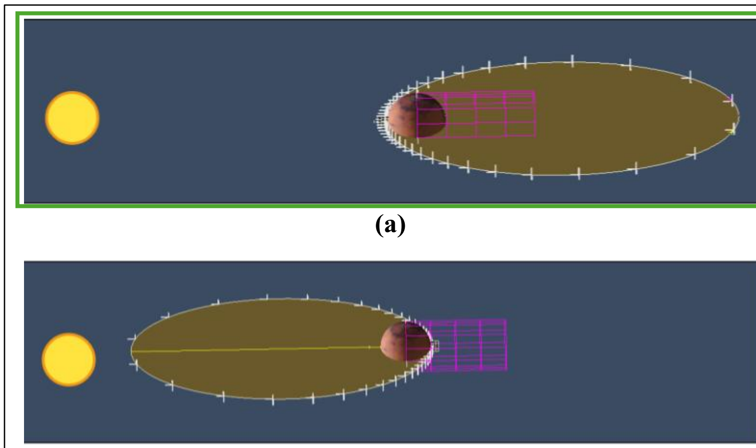

(a)

(b)

Figure 13. Opposite extreme orbit orientations, modeled with 0° beta angle at 1-Sol Mars orbit for: (a) Periapsis on Sun side (identified to represent worst-case). (b) Apoapsis on Sun side.

3.3.2.3 Venus Flyby

The Venus flyby modeling method is highlighted in this section as this mission location consists of a trajectory rather than an orbit. To model this, two methods were used.

The first method used a sample trajectory that was provided by the Systems Analysis and Concepts Directorate (SACD) at NASA Langley Research Center. For this model, only "edge to planet" and "edge to Sun (horizontal)" were analyzed. Only these two radiator orientations were modeled for the Venus flyby sample trajectory because maintaining edge to major environmental heating sources is advantageous while the reactor is powered ON. Otherwise, the reactor and PCS would need to be throttled down to reduce the internally generated heat load so the components do not exceed their limits. The second method was built to measure incident environmental heating at positions at finite altitudes to Venus. Rather than a sample trajectory, the intent of this model is to compare environmental sink temperatures at arbitrary trajectory points. This method is included because it is independent of a sample trajectory.

These two methods are illustrated in Figure 14 for the “edge to Sun (horizontal)” panel orientations. At the end of the sample trajectory provided, the vehicle is at an altitude of 6000 km. This altitude is highlighted as a red line at 6000 km in the graph in Figure 14b for comparison between the two models.

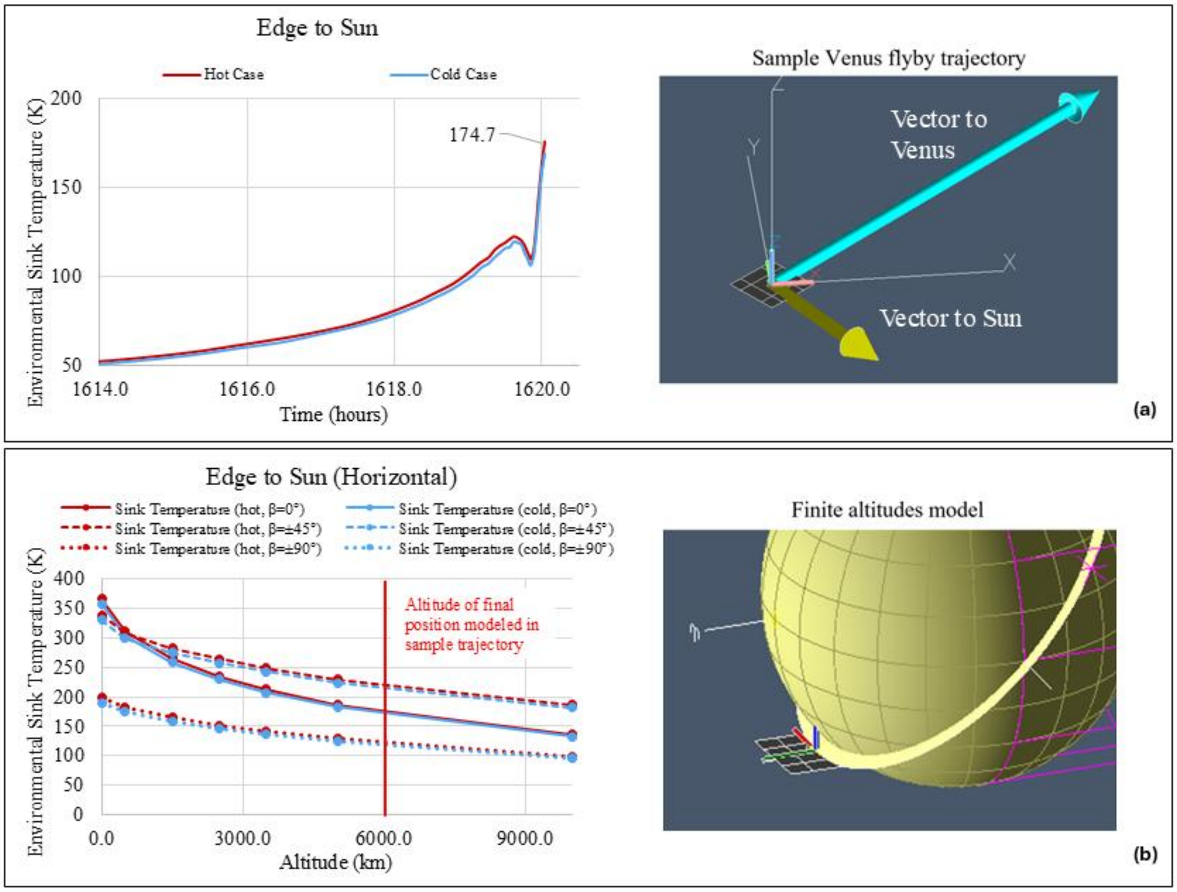

Figure 14. The two methods used for modeling Venus flyby are described:
(a) Venus trajectory, and (b) finite altitudes model.

3.3.2.4 Interplanetary Travel

In addition to the mission locations, the thermal environment of interplanetary space must be considered. The temperature of deep space is approximately 2.7 K (Appendix A.1). Therefore, the minimum T_∞ is ~2.7 K across the entire mission, occurring when the panel is distant from all celestial bodies and oriented “edge to Sun”.

3.4 Reduction of Cases to Capture the Thermal Environment

From the T_∞ and R_c curves generated from the TD model and data analysis step in Excel, the cases were then reduced from the initial 328 cases. The cases were reduced first by selecting ideal panel orientations for the mission and then by identifying enveloping beta angles. The reduced set of bounding cases will significantly reduce data processing time in future thermal analysis that includes the full radiator or NEP vehicle model. The envelope of T_∞ and R_c values from the reduced set of cases is presented in Table 3 in Results (Section 4), and a complete list of all the selected cases is provided in Table 12 in Appendix D. Summary of Selected Cases.

First, the ideal panel orientations were identified. This selection results in the actual reduction of panel orientations to be considered for the mission. The selected panel orientations are, most importantly, compatible with reactor power states at each mission location relative to the mission phase (e.g., commissioning or reactor powered ON at steady state). The reactor will be powered OFF prior to commissioning and reactor startup, where LEO 500 km, LEO 1100 km, and NRHO are possible options. For this power state, ideal environmental sink temperatures are high to prevent freezing of the internal working fluids. Phases analyzed for the reactor powered ON include NRHO, Mars orbits, the Venus flyby, and Interplanetary travel. For this power state, ideal environmental sink temperatures are low to maximize heat rejection capability. The selected panel orientations were also those with greater consistency in T_∞ and R_c values across the completion of one orbit and across the beta angle sweep. From a thermal control perspective, orientations that have greater consistency are more ideal than orientations which see large variations. Where one or more panel orientations are not clearly identifiable as ideal or non-ideal, they were included for continued analysis under future thermal analysis studies.

Once the panel orientations are selected, the case set can be further simplified by identifying the beta angles that represent the hottest or coldest cases to capture the extrema of thermal environment. While panel orientation selection provides recommendations for the mission, the selection of beta angles simplifies the number of cases necessary for future modeling. The beta angles selected at each panel orientation must a) include the temperature extremum for that panel orientation, and b) represent the highest or lowest sink temperature throughout the orbit. If a beta angle includes both criteria, only one beta angle was selected to be representative of a hot or cold case. A beta angle case may also be selected for modeling if it represents any significant thermal characteristics such as rapid change in environmental sink temperature or a long eclipse duration.

4 Results

There were 328 total cases run with the TD model, due to the combinations of locations, panel orientations, beta angles, and hot/cold case specifications. All resulting environmental sink temperature and heat rejection capability curves for each mission location are included in Appendix E.

By selecting ideal panel orientations for each location, the cases were reduced from 328 cases to 35 cases. The summary of selected ideal panel orientations at each mission location, and selected beta angles for simplified modeling, is provided in Appendix D.

For the target application, the environmental sink temperature while the reactor is powered OFF ranges from 30 K to 353 K, and while the reactor is powered ON ranges from 2.7 K to 243 K. A summary of the results is provided in Table 3.

Table 3. Reactor Power State with Corresponding Thermal Environment Extrema.

Reactor Power State	Objective	Case	T_∞ [K]	Location (specification)	Panel Orientation
Powered OFF	Maximize radiator panel temperature, prevent freezing	Hot	353	LEO (500 km, 0˚ beta angle)	Face to Earth (Edge to VV)
					Face to Sun
		Cold	30	NRHO (9:2 lunar synodic resonant, southern L2 Langrangian point, 0˚ beta angle)	Face to Sun
Powered ON	Minimize radiator panel temperature, prevent overheating, increase heat rejection	Hot	243	Mars orbit (<1-, 1-, 2-, 5-, 10-Sol, 250 km perigee, 45˚ beta angle)	Edge to Sun (horizontal)
		Cold	2.7	Interplanetary Travel	Edge to Sun

5 Discussion

Analysis and selection between the ideal panel orientations is outlined in Section 5.1. Section 5.2 includes a discussion of rapid changes in environmental sink temperature that were identified in the study.

After the selection of panel orientations, and enveloping beta angles representative of hot and cold cases were selected for further simplification of the model for future vehicle model thermal analysis. With the selection of enveloping beta angles, the number of cases was reduced to 35. The selected beta angles and justifications for selection are summarized in Appendix D, in Table 13 and Table 14. This reduced set of cases is the minimum number of cases required for future modeling that captures the variety of space environments and thermal environment extrema.

5.1 Selection of Ideal Panel Orientations

Described in this section is the process of selecting ideal panel orientations for each mission location. A final list of the selected panel orientations is provided in Appendix D, Table 12 to summarize the selections made in this section. Analysis of ideal panel orientations for LEO 500 km, LEO 1100 km, and NRHO is conducted for two different reactor states, when the reactor is powered ON or OFF. For Mars orbits, Venus flyby, and interplanetary travel mission locations, the analysis considers only periods when the reactor is powered ON.

5.1.1 LEO 500 km and 1100 km

LEO 500 km and 1100 km have the same panel selections, and both altitudes were analyzed for reactor power states ON and OFF. While both power states were analyzed for completeness, it is important to note that LEO 1100 km is the minimum orbit for nuclear safe operations [25]. For LEO orbits, the ideal panel orientation was "edge to Sun (horizontal)" when the reactor is powered ON, and "face to Earth (edge to VV)" and "face to Sun" when the reactor is powered OFF.

For both reactors powered ON and powered OFF cases, the "edge to earth (edge to VV)" panel orientation was eliminated from future analysis as there was significant variability in environmental sink temperatures and rejection capability across the beta angle sweep.

When the reactor is powered ON, ideal panel orientations are those that expose the panels to the lowest environmental sink temperatures to maximize heat rejection capability. The "edge to Sun (horizontal)" and "edge to Sun (vertical)" panel orientations have lower average temperatures and greater consistency across beta angles and the duration of the orbit compared to all other panel orientations. The "edge to Sun (vertical)" orientation was selected for the reactor powered ON state because it provided a lower average environmental sink temperature when compared to "edge to Sun (horizontal)".

When the reactor is powered OFF, the remaining orientations include "face to Earth (edge to VV)", "edge to Earth (edge to VV)", and "edge to Earth (face to VV)". Of these orientations, both "face to Earth (edge to VV)" and "face to Sun" have higher environmental sink temperatures which align with requirements of high environmental sink temperature for the candidate commissioning orbits. Between these two panel orientations, the advantages are unclear based on thermal environment analysis alone. The "face to Sun" orientation has the advantage of higher average temperatures, but there was a significant change in environmental sink temperatures when traveling into Earth's shadow, while the "face to Earth (edge to VV)" orientation has the advantage of less rapid change in environmental sink temperature over time, but lower temperatures compared to "face to Sun". Thus, the "face to Earth (edge to VV)" and "face to Sun" orientations were selected for further analysis in upcoming full vehicle thermal model studies.

5.1.2 NRHO

Because NRHO is also a possible commissioning orbit, ideal panel orientations for both the reactor powered ON and OFF states were identified for this orbit. First, a few panel orientations were eliminated for both reactor states due to large variation in T_∞ and R_c values across the beta angle sweep, and consistency of these values is ideal (see Section 3.4). The eliminated panel orientations include "edge to Moon (edge to VV)", "edge to Moon (face to VV)", and "face to Moon (edge to VV)". For "edge to Moon (edge to VV)", and "edge to Moon (face to VV)" orientations, there was a sink temperature difference of ~260 K between the 0˚ beta angle to the 45˚ beta angle cases while the panel is away from the Moon (which is most of the orbit duration in NRHO). There was also significant variation in sink temperature as a function of beta angle for the "face to Moon (edge to VV)" case, with the most extreme difference between 0˚ beta angle to the 45˚ beta angle cases around 200 K. The remaining panel orientations have more consistency across T_∞ and R_c values and were selected next based on reactor power states.

When the reactor is powered ON, ideal orientations include "edge to Sun (horizontal)" and "edge to Sun (vertical)". Between these two orientations, the "edge to Sun (vertical)" panel orientation was selected due to lower average and maximum environmental sink temperatures throughout the orbit.

When the reactor is powered OFF, the remaining panel orientation with the highest overage sink temperature was the "face to Sun" orientation. Despite a 0˚ beta angle case at this panel orientation, the vehicle passes through the Moon's shadow and experiences a rapid change in environmental sink temperature which is not ideal (See Section 3.3.2.1.1 for discussion of cylindrical shadow approximation and Section 5.2.1 for discussions on rapid temperature change for NRHO eclipse case). Nonetheless, this orientation was selected due to highest environmental sink temperatures across all beta angles throughout most of the orbit.

5.1.3 Mars Orbits

For all Mars orbits, the reactor will be fully powered ON, so the ideal panel orientations have low environmental sink temperatures to maximize heat rejection capability. The “face to Mars (edge to VV)”, “edge to Mars (edge to VV)”, and “edge to Mars (face to VV)” panel orientations are eliminated due to the high variability in environmental sink temperature across the beta angles. Additionally, the “face to Sun” orientation was eliminated due to the high environmental sink temperatures throughout the whole orbit. Between “edge to Sun (horizontal)” and “edge to Sun (vertical)”, the “edge to Sun (horizontal)” panel orientation was selected due to the lower overall environmental sink temperatures throughout the orbit.

5.1.4 Venus Flyby

For the Venus flyby, two different radiator panel orientations were analyzed: “edge to Venus (horizontal)” and “edge to Sun” orientations. The “edge to Sun” orientation was selected as ideal because the maximum environmental sink temperature was lower for this orientation when compared to that of the “edge to Venus (horizontal)” orientation. Furthermore, the environmental sink temperature was more consistently low throughout the trajectory and closest pass for this panel orientation.

5.1.5 Interplanetary Travel

The reactor will be powered ON during interplanetary travel. The ideal panel orientation was “edge to Sun” to minimize radiative flux. With no incident solar flux, the environmental sink temperature is ~2.7 K (Sec. 3.3.2.4).

5.2 Rapid Changes of Environmental Sink Temperature

The analysis of environmental sink temperatures reveals a significant consideration of rapid changes of environmental sink temperature, often most pronounced in elliptical orbits. This occurs when the vehicle passes the periapsis for a short period of time, but experiences large increase in the incident solar and IR flux due to increased OLR and albedo flux from passing near the celestial body. The most significant temperature gradient for the reactor powered ON is described in Figure 15.

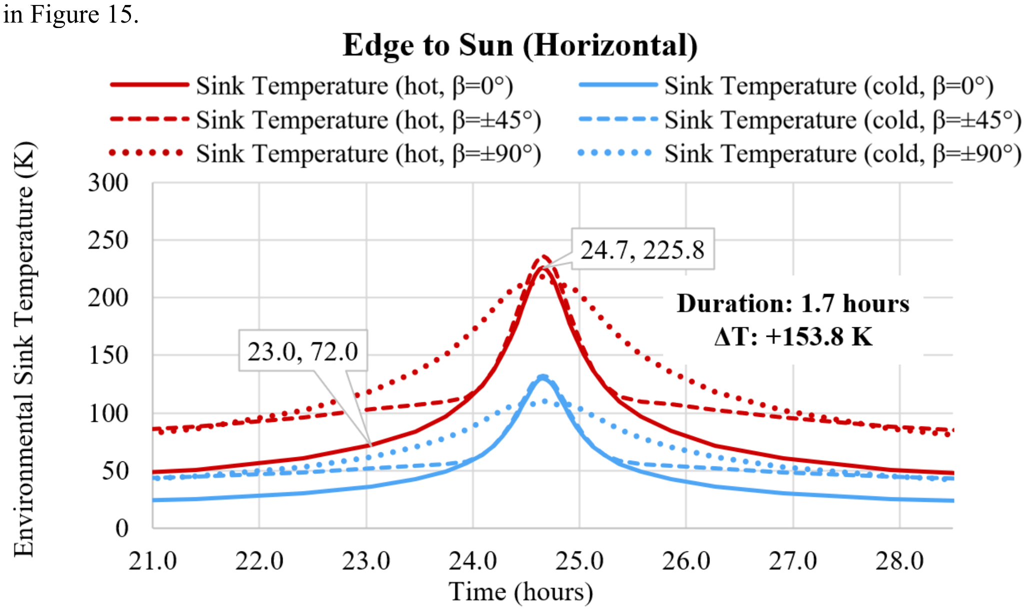

Figure 15. Most rapid change in environmental sink temperature for reactor powered ON. Mars 10-Sol orbit edge-to-Sun panel orientation.

The most significant environmental sink temperature change over time while the reactor was powered ON was at the Mars 10-Sol orbit. There was a 153.8 K increase in environmental sink temperature over 1.7 hours when approaching the point of periapsis.

5.2.1 Limitations in Identifying Rapid Change in Environmental Sink Temperature Due to Cylindrical Shadow Approximation

It is important to note that the trends with respect to time for entering and exiting planetary shadow were limited by the model set up, due to the cylindrical shadow model used in this study. Due to the cylindrical shadow model, the changes would be instantaneous, and the "rate of change" for shadow entry and exit was due to the discretization of the orbit, not a physical phenomenon. Instead, there may be a more gradual change in environmental sink temperature due to passing through the penumbra region of the eclipse. Therefore, while trends show extrema throughout the orbit for environmental sink temperatures, and the maximum and minimum values are represented on the graphs with corresponding times, the detailed temperature profiles are limited by the model and should be regarded as approximations.

6 Conclusion and Future Work

The objectives met within this study support future research efforts within the MARVL project and Space Nuclear Propulsion portfolio. First, the thermal environments of all locations for the target mission have been defined and can be used to support future analysis. Next, the study of LEO and NRHO mission locations will help inform optimal orbits for reactor commissioning. In addition, the number of cases required for future analysis has been reduced from 328 to 35 cases based on thermal driving cases for each mission location. This is impactful as the TD model will be used for future full vehicle model studies to analyze the effect of radiative interaction between the vehicle and radiator panels. Finally, the quantification of environmental sink temperatures and identification of rapid change in environmental sink temperature over time is useful for predicting component transient properties and the performance of more sensitive equipment with low thermal time constants.

Future work is needed for more accurate modeling of the temperature gradient for vehicle passage through shadow, as the current study uses a cylindrical approximation for the eclipse cases. Future work is also needed to understand the NRHO long duration eclipse risk. The Gateway NRHO Earth shadow passes are limited to two from 2024-2038, so more information is needed for the target mission which has a 2039 Earth departure and ~3-year mission duration.

Future work is needed for the selection and evaluation of optical properties of composite material for the radiator panel face sheets. Testing of these materials will be useful especially to identify optical properties within the temperature range of interest. To reflect future material property analysis, the optical property assumptions will be updated in the Excel model to identify environmental sink temperature and heat rejection capability curves for updated optical property assumptions

The model generated in this study captures the effects of view factor and location to measure the thermal environment by using a representative 1 m x 1 m panel with parameterized optical properties and radiator temperature. The model may serve as a useful tool for further MARVL analysis, and the techniques used in this paper can be applied to other conceptual design-level mission surveys of radiator performance or other thermal performance metrics, which may aid in analysis for future mission concepts.

Acknowledgements

The authors acknowledge the support of Emanuel Gruella and Jaycie Hall at Analytical Mechanics Associates and Kimberly Martin and Alexander Scammell at NASA Langley Research Center in preparation of this publication, Jonah Smith at Amentum for insight and discussion on Gateway NRHO modeling techniques, and NASA intern Diego Perea for contributions to thermal environment analysis. Additionally, we appreciate the programmatic and technical support provided by the NASA Space Nuclear Propulsion project. Finally, we extend a special thank you to Dr. Julia Cline at NASA Langley Research Center for the incredible mentorship and support throughout this research. The MARVL project is funded by the Space Technology Mission Directorate (STMD) Early Career Initiative program.

References

[1] NASA Engineering and Safety Center, "Independent Assessment of the Technical Maturity of Nuclear Electric Propulsion (NEP) and Nuclear Thermal Propulsion (NTP) Systems," Marshall Space Flight Center, 2020.

[2] National Academies of Sciences, Engineering, and Medicine, "Space Nuclear Propulsion for Human Mars Exploration," National Academies Press, Washington D.C., 2021.

[3] K. Polzin *et al.*, "SNP-PLAN-0043 Space Nuclear Propulsion (SNP) Technology Maturation Plan for High Power Nuclear Electric Propulsion, Version 1.1," NASA Space NUclear Propulsion Project, Huntsville, 2026.

[4] L. Forsley, T. Benyo, P. Mosier-Boss and L. Dudzinski, "An Extremely High Isp Spacecraft Propulsion System," in *American Nuclear Society NETS-22*, Cleveland, OH, 2022.

[5] B. Mattfeld, C. Stromgren, H. Shyface, D. R. Komar, W. Cirillo and K. Goodliff, "Trades Between Opposition and Conjunction Class Trajectories for Early Human Missions to Mars," in *Space 2014*, San Diego, CA, 2014.

[6] M. Duchek *et al.*, "Hybrid NEP-Chemical Vehicle and Propulsion Technology Study for Crewed Mars Missions," in *68th JANNAF Propulsion Meeting*, Virtual, 2021.

[7] P. R. Chai, R. G. Merrill and M. Qu, "End-to-End Trajectory for Conjunction Class Mars Missions Using Hybrid Solar-Electric/Chemical Transportation System," in *AAS/AIAA Space Flight Mechanics Meeting*, Napa, CA, 2016.

[8] W. M. Kimmel *et al.*, "Technology Readiness Assessment Best Practices Guide," 2020.

[9] W. Machemer, M. Duchek and D. Nikitaev, "Considerations for Radiator Design in Multi-Megawatt Nuclear Electric Propulsion Applications," in *AIAA SciTech Forum and Exposition*, National Harbor, MD, 2023.

[10] M. Duchek *et al.*, "Key Performance Parameters for MW-Class NEP Elements and their Interfaces," in *ASCEND*, Las Vegas, 2022.

[11] M. Duchek, M. Clark, A. Pensado, C. Harnack, W. Machemer and E. Grella, "Sensitivity of Hybrid NEP-Chemical Vehicle Mass to Assumptions for Crewed Opposition-Class Mars Missions," in *AIAA Propulsion and Energy Forum*, Virtual Event, 2021.

[12] A. J. Juhasz, "An Analysis and Procedure for Determining Space Environmental Sink Temperatures With Selected Computational Results," in *Environmental Systems*, Toulouse, France, 2000.

[13] D. Gilmore, Spacecraft Thermal Control Handbook, Volume I: Fundamental Technologies, El Segundo, California: The Aerospace Press, 2002.

[14] B. D. Hamill, R. G. Schunk and L. Erickson, "Human Landing System Lunar Thermal Analysis Guidebook," Marshall Space Flight Center, 2021.

[15] B. C. Roberts, "SLS-SPEC-159 Cross-Program Design Specification for Natural Environments (DSNE) Revision G," Marshall Space Flight Center, 2019.

[16] E. Zimovan-Spreen, S. Scheuerle, B. Mccarthy, D. Davis and K. Howell, "Baseline Orbit Generation for Near Rectilinear Halo Orbits," in *AAs/AAIA Astrodynamics Specialist Conference*, Big Sky, MT, 2023.

[17] J. Smith, "Gateway PTCS Integrated Thermal Math Model," in *International Conference on Environmental Systems*, Virtual, 2020.

[18] M. Qu, R. G. Merill, P. Chai and D. R. Komar, "Optimizing Parking Orbits for Roundtrip Mars Missions," in *2017 AAS/AIAA Astrodynamics Specialist Conference*, Stevenson, WA, 2017.

[19] V. L. Pisacane, The Space Environment and Its Effects on Space Systems, American Institute of Aeronautics and Astronautics, Inc., 2008.

[20] G. C. Tuan *et al.*, "Evaluation of Coatings and Materials for Future Radiators," *SAE Transactions,* vol. 115, pp. 83-94, 2006.

[21] R. L. Broeren, "Radiator Wing Rotation Algorithm Overview for the International Space Station's External Active Thermal Control System," *SAE Transactions,* vol. 107, pp. 826-844, 1998.

[22] L. Carrillo, D. Farner and C. Preston, "NASA-TFAWS Short Course ISS Payload Thermal Environments," 2015.

[23] D. E. Lee, "White Paper: Gateway Destination Orbit Model: A Continuous 15 Year NRHO Reference Trajectory," Johnson Space Center, 2019.

[24] S. Rickman, "Introduction to Orbital Mechanics and Spacecraft Attitudes for Thermal Engineers," in *Thermal and Fluids Analysis Workshop*, Moffett Field, CA, 2025.

[25] S. R. Oleson *et al.*, "Compass Final Report: Nuclear Electric Propulsion (NEP)- Chemical Vehicle 1.2," Glenn Research Center, 2021.

[26] J. Silk, "The Cosmic Microwave Background Radiation," in *The Infrared and Submillimetre Sky After COBE; Proceedings of the NATO Advanced Study Institute*, Les Houches, France, 1991.

Appendices

Appendix A. Thermal Environment Specification for Relevant Phases

Thermal values for direct solar radiation, albedo, and OLR are defined for LEO, NRHO, LDHEO, Mars orbits, and the Venus flyby. Orbital parameters for planetary bodies will be derived from values presented in the Spacecraft Thermal Control Handbook [13] and cross-checked with built in values found in Thermal Desktop. Summary tables for direct solar, albedo, and OLR will be included for each mission location, and report values that include uncertainty to capture worst-case hot and cold.

To calculate the extrema for direct solar radiation, the minimum and maximum distance of the vehicle at each phase from the Sun in astronomical units (AU) is used (Table 4).

Table 4. Select orbital parameters.

	Closest Distance to Sun [AU]	Furthest Distance to Sun [AU]
Earth	0.9833	1.0167
Moon	0.9809	1.0194
Mars	1.381	1.666
Venus	0.7184	0.7282

Then, the direct solar radiation intensity is calculated using the following Equation A1:

$$Solar\ Flux = \frac{1}{d^2} \times 1367\ W/m^2 \quad \text{(A1)}$$

Where d is the distance in AU, and $1367\ W/m^2$ is the solar constant at 1 AU. Figure 16 illustrates how the solar flux value decreases with distance from the Sun using the orbit semimajor axis for various planets.

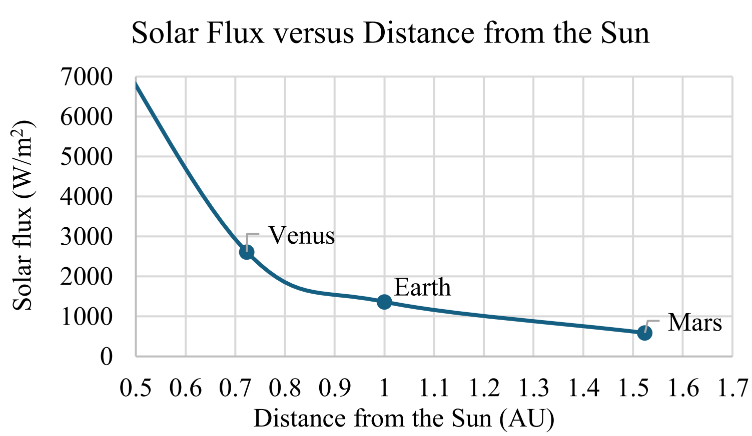

Figure 16. Solar flux as a function of distance from the Sun.

The trajectory profile of a 2039 NEP/chemical Mars opposition class mission has been delivered by trajectory subject matter experts from Langley SACD to obtain specific positions of the spacecraft in a Sun centered reference frame. This trajectory is based on initial estimates for launch date and NEP vehicle capabilities. From this trajectory profile, the distance between the NEP vehicle and the Sun will vary from a minimum of 0.5955 AU to a maximum of 1.6510 AU. Figure 17 illustrates this trajectory.

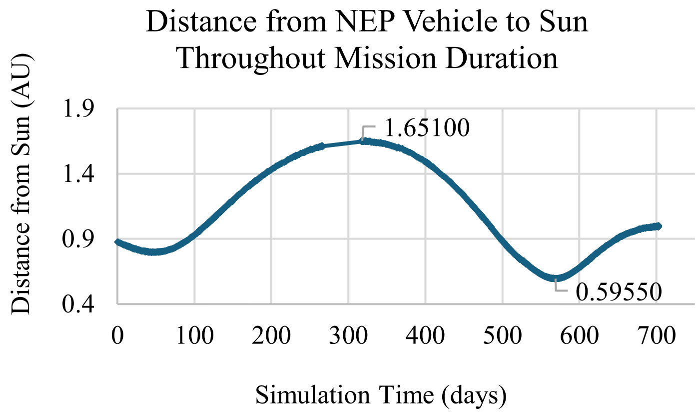

Figure 17. Spacecraft distance from the Sun in AU throughout mission duration for a sample trajectory. Note: The trajectory profile is plotted for a sample Mars mission and is subject to change. Minimum and maximum direct solar radiation values based on trajectory profiles must be updated if changes are made to the trajectory.

According to the sample mission trajectory plotted in Figure 17, the minimum distance of the spacecraft to the Sun is 0.59550, closer than Venus' perihelion distance. When substituting this value into Equation A1, the maximum direct solar radiation calculated for this mission is 3,855 W/m^2.

The maximum direct solar radiation must be estimated using the sample trajectory in Figure 17, since the closest the spacecraft will travel to the Sun will likely be closer than the perihelion distance of Venus. Regarding the cold case environment, a wider envelope to account for variation in the specific spacecraft path is presented in this document. Direct solar radiation will be at a minimum of 492.51 W/m^2 at Mars' aphelion distance (Section A.5, Table 10).

A.1 Interplanetary Travel

When the spacecraft is in interplanetary travel with no view factor to the sun, there will be a minimum temperature of approximately 2.7 K due to the cosmic microwave background [26].

A.2 Low Earth Orbit

Values defined in this section for LEO apply to 500 km and 1100 km altitudes.

Earth's orbit has a perihelion of 0.9833 AU and aphelion of 1.0167 AU. Earth has a 23.44° tilt. For both 500 km and 1100 km LEO in the mission, the spacecraft will have a 28.5° inclination angle. The solar beta angle will vary throughout the Earth orbit between -51° and +51°. With the movement of Earth between perihelion and aphelion, the direct solar thermal radiation will vary between a minimum of 1,322 W/m^2 and a maximum of 1,414 W/m^2, with an average of 1,367 W/m^2 at 1 AU [13, p. 22].

Hot case and cold case values for direct solar radiation, albedo, and OLR are summarized in Table 5 [13].

Table 5. LEO extreme-case thermal environments.

Case	Direct Solar [W/m^2]	Albedo	OLR [W/m^2]
Hot Case	1414	0.22*	331
Cold Case	1322	0.40*	150

**Albedo Correction*: Albedo values must be corrected according to beta angle to account for non-Lambertian reflection near the terminator [13, p. 27]. Orbit-average albedo correction is applied to the albedo values for both hot and cold cases. The corrections for the following beta angles are applied:

Beta Angle	Albedo Correction
0°	+0.04
±25°	+0.05
±52°	+0.09

The inputs for albedo and OLR extrema are identified according to the following classifications:

Time Constants: For worst-case analysis, the shortest measured time constant of 16-seconds has been used for selection. This precision was selected to account for equipment sensitivities to fluctuations in albedo and IR, since applicable equipment will have relatively low thermal time constants.

Material sensitivity: Current optical property assumptions for MARVL radiator panels are $\alpha_s = 0.7$ and $\varepsilon_{IR} = 0.85$ (Section 3.1). Optical property assumptions may vary slightly, but overall the radiator panel material is assumed to be both IR and albedo sensitive. However, if solar absorptivity assumptions lower significantly, these input values must be updated to instead reflect material sensitivity to IR only [13, pp. 26-27].

Inclination angle: With a 28.5° inclination angle, extremes are bound with data for 0-30 inclination angle values [13, pp. 26-27].

Error: The reported albedo and OLR values in Table 5 are a conservative (3.3-σ) set of recommended values that will be exceeded 0.04% of the time. The alternative set of values presented in the Spacecraft Thermal Control Handbook is less-severe (2-σ) values that will be exceeded 5% of the time. The 3.3-σ values are used here to represent worst-case thermal environments.

A.3 Near-Rectilinear Halo Orbit

Vehicles in the 9:2 Lunar Synodic Resonant Near-Rectilinear Halo Orbit (NRHO) have a minimum perilune of 1,458 km and maximum apolune of 70,112 km [17, p. 5]. The Moon varies in distance from Earth with a perigee of 363,300 km and apogee of 405,500 km [14]. The distance from the Moon to the Sun varies from a perihelion of 0.9809 AU and an aphelion of 1.0194 AU. The solar beta angle varies in this orbit between -90˚ and +90˚. The argument of periapsis is nominally 90˚. However, the Moon's equator has a ±1.54˚ tilt with respect to the ecliptic plane, and an additional ±3 is applied to account for oscillations estimated in 9:2 NRHO. A Keplerian approximation is used for NRHO, and the orbital parameters for this approximation are provided in Table 6 [14].

Table 6. Orbital parameters for NRHO Keplerian approximation.

Orbital Parameter	Beta 0˚	Beta ±45˚	Beta ±90˚
Orbit Inclination	90	90	90
Right Ascension of the Ascending Node (RAAN)	270	270	90
Argument of Periapsis	85.46	85.46	85.46
Right Ascension of the Sun (RAS)	270	225	0
Right Ascension of the Prime Meridian	0	0	0

Hot case and cold case values for direct solar radiation, albedo, and OLR for NHRO are summarized in Table 7.

Table 7. NRHO extreme-case thermal environments.

Extrema	Direct Solar [W/m^2]	Albedo	OLR [W/m^2]
Maximum	1426	0.20	285
Minimum	1310	0.07	91

Note: For thermal modeling with enveloping environments [14, pp. 18-19], analysis uses the subsolar coordinate system.

Direct solar radiation values are defined below [15, pp. 200-201]:

Maximum direct solar: 1,421 W/m^2
Minimum direct solar: 1,315 W/m^2

With a +/-5 W/m^2 measurement uncertainty when values are used in thermal analysis.

The landscapes of the near side (Earth-facing side) of the Moon and far side lead to significant variation in thermal characteristics. The near side of the Moon has an abundance of maria while the far side is composed of mostly highlands. The breakdown of albedo and OLR values for the near side and far side are described below [15, p. 201], with albedo values included for the lunar south pole [15, p. 276].

Near Side
mean albedo: 0.12, ranging from 0.07 to 0.2
mean IR: 164 W/m^2 ranging from 91-285 W/m^2

Far Side
mean albedo: 0.15, with variation of +/-0.05
mean IR: 154 W/m^2, ranging from 131-285 W/m^2

South Pole
Mean albedo: 0.16

A.3.1 NRHO Eclipse Case

Another consideration for the NRHO is the duration the spacecraft will spend with no direct solar radiation which could result either from its position in Earth's shadow or the Moon's shadow.

Passage through Earth's shadow can last longer than 90 minutes without mindful trajectory design. This is because Earth's shadow is larger than the Moon's shadow size as a spacecraft would observe at the NRHO position, and spacecraft passage through Earth's shadow is typically longer duration due to lower orbital velocity away from perilune where Earth's shadow usually occurs in NRHO [16, p. 4]. The NASA Gateway 9:2 Lunar Synodic Resonant NRHO was selected to avoid eclipses by the Earth from January 2020 to February 2035, with only two partial eclipses occurring in 2034 and 2035 [14] [23]. Passage through Earth's shadow for a vehicle in this orbit can be avoided with orbital modifications.

Passage through the Lunar shadow will be a maximum of 76.1 minutes, with 73.2 minutes in totality for the Gateway NRHO. Values from Table 8 are used to identify worst case eclipse durations.

Table 8. Duration in lunar shadow for Gateway 9:2 Lunar Synodic Resonant NRHO [14].

Shade	Minimum [minutes]	Mean [minutes]	Maximum [minutes]
Penumbra	0.9	52.5	76.1
Umbra	10.2	49.9	73.2

A.4 Lunar Distant High Earth Orbit

Direct solar radiation for the Lunar Distant High Earth Orbit (LDHEO) is calculated using the closest and farthest distance from the Sun in AU with Equation A1. The values for Earth's perihelion and aphelion distances are defined in Section A.2. This calculation yields the following values for maximum and minimum direct solar radiation:

Maximum direct solar: 1,421 W/m^2

Minimum direct solar: 1,322 W/m^2

Albedo and OLR values for the LDHEO align with values for LEO found in Section A.2. Consideration in modeling must be made to adjust for the spacecraft's altitude away from Earth. The LDHEO has a perigee of 407 km and an apogee of 400,000 km [7].

A.5 Mars Orbits

Mars has a 25.19° planetary tilt and has a perihelion of 1.381 AU and aphelion of 1.666 AU. One Mars sol is equal to 88775.244 seconds.

Based on previous mission trajectory studies, the spacecraft's orbit around Mars is constrained by a perigee of 250 km [7]. The various orbits in consideration range from a ~0.215-Sol orbit with an apogee altitude of 7,660 km [18] to a 10-Sol orbit with an apogee altitude of 182,000 km. The <1-Sol orbit is specified at an inclination angle of 88° [5], but for all other Mars orbits the inclination angle, not yet specified, will range between 0° and 180° [3, 19]. The solar beta angle will vary between -90° and +90° for all Mars orbits. A summary of these orbits is shown in Table 9.

Table 9. Summary of Martian-Phase Orbits.

Orbital Period	Orbit Inclination [°]	Perigee Distance [km]	Aphelion Distance [km]
<1-Sol	88	250	7660
1-Sol	0-180	250	33867
2-Sol	0-180	250	57573.4
5-Sol	0-180	250	115000
10-Sol	0-180	250	182000

Direct solar radiation for the Martian Orbits is calculated using Mars's perihelion and aphelion values, and albedo and OLR values were defined in [13, p. 56]; these values are reflected in Table 10.

Table 10. Martian Extreme-Case Thermal Environment [13]

Extremum	Direct Solar [W/m^2]	Albedo	OLR [W/m^2]
Maximum	716.77	0.28	470
Minimum	492.51	0.17	30

A.6 Venus Flyby

Venus's orbit around the Sun varies with a perihelion distance of 0.7184 AU, and an aphelion distance of 0.7282 AU [13, p. 49]. The direct solar radiation, albedo, and OLR values are defined in [13, pp. 52-53]. These values are summarized in Table 11.

Table 11. Venus Extreme-Case Thermal Environment [13]

Extremum	Direct Solar [W/m^2]	Albedo	OLR [W/m^2]
Maximum	2759	.82	178.4
Minimum	2650	.78	146.3

Appendix B. Comparison of Modeling Periapsis vs. Apoapsis on Sun-Side of Mars

For eccentric orbits, the direction of the major and minor axis on eccentric orbits can rotate the ellipse within the same plane. However, altering the direction the point of periapsis is located relative to the Sun will affect thermal loads. As this specification is not yet detailed for the target mission, the study must consider all possibilities. The goal of this analysis is to determine what conditions yield the worst-case conditions; thus, all eccentric orbits will be oriented accordingly. To determine which orientation of the eccentric orbits will capture the extrema of hot and cold environments, two extreme opposite orientations were analyzed. The two cases modeled for this analysis are shown in Figure 18. For this analysis, the 1-Sol Mars orbit was modeled, panel orientation "edge to Sun (horizontal)".

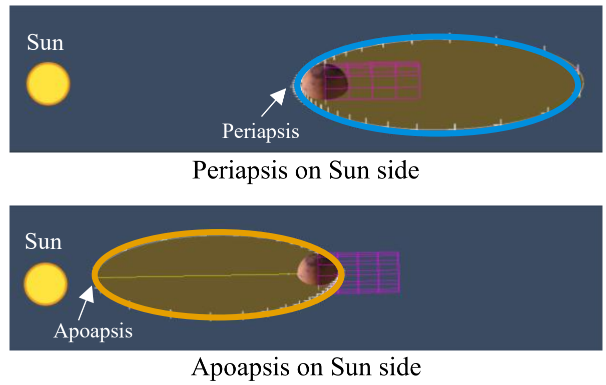

Figure 18. Modeled cases for identifying worst case orientation of eccentric orbits.

Environmental sink temperature (Figure 19) and heat rejection capability (Figure 20) curves are shown for both hot and cold cases. Optical properties used in this analysis are α = 0.3 and ε = 0.85. Point of periapsis or apoapsis on Sun side is notated P-to-Sun and A-to-Sun respectively.

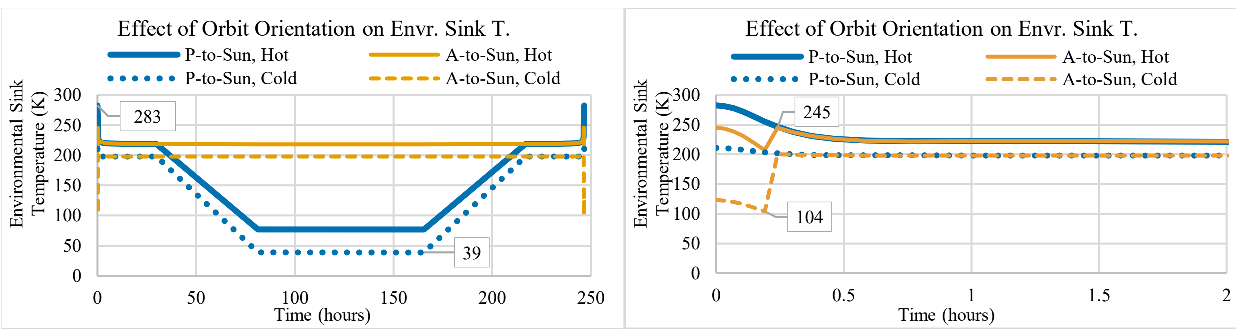

(a) **(b)**

Figure 19. Environmental sink temperature curves for orbit orientation analysis. (a) Complete orbit. (b) Magnified view of first two hours of orbit, on the Sun side.

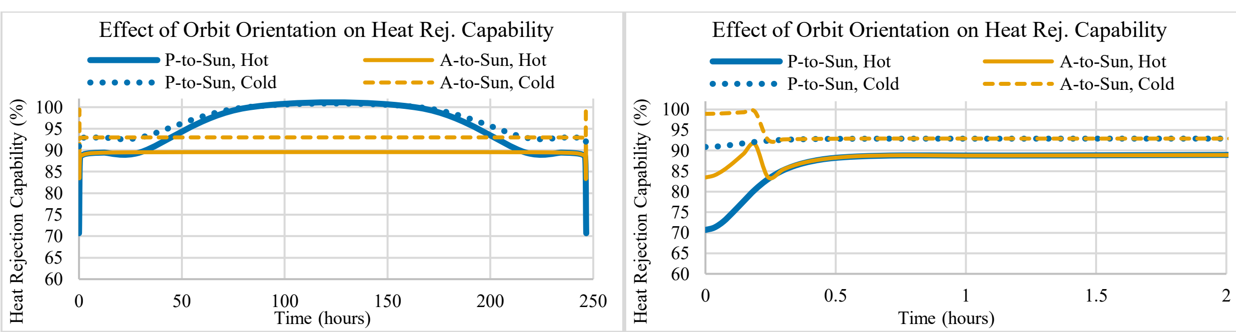

(a) **(b)**

Figure 20. Heat rejection capability curves for orbit orientation analysis. (a) Complete orbit. (b) Magnified view of first two hours of orbit, on the Sun side.

For this analysis, environmental sink temperature ranges for periapsis on Sun side and apoapsis on Sun side are 39 K to 283 K and 104 K to 245 K respectively. These data points are labelled in Figure 19a and Figure **19**b. Thus, for orbits with the periapsis on the Sun side (P-to-Sun) (the apoapsis is away from the Sun), absolute maximum and minimum environmental sink temperatures are reached. Therefore, eccentric orbits are modeled in this study with the periapsis on the Sun side. This includes 0° and 45° beta angles for NRHO, and 0° and 45° beta angles for Mars orbits.

Appendix C. Modeling Multiple Sequential Orbits

Multiple sequential orbits were run for Mars 1-Sol orbits to verify that the model is consistent after multiple runs. For this analysis, optical property inputs of $\alpha = 0.3$ and $\varepsilon = 0.85$ were used. As observed in Figure 21, a constant cyclic pattern is maintained.

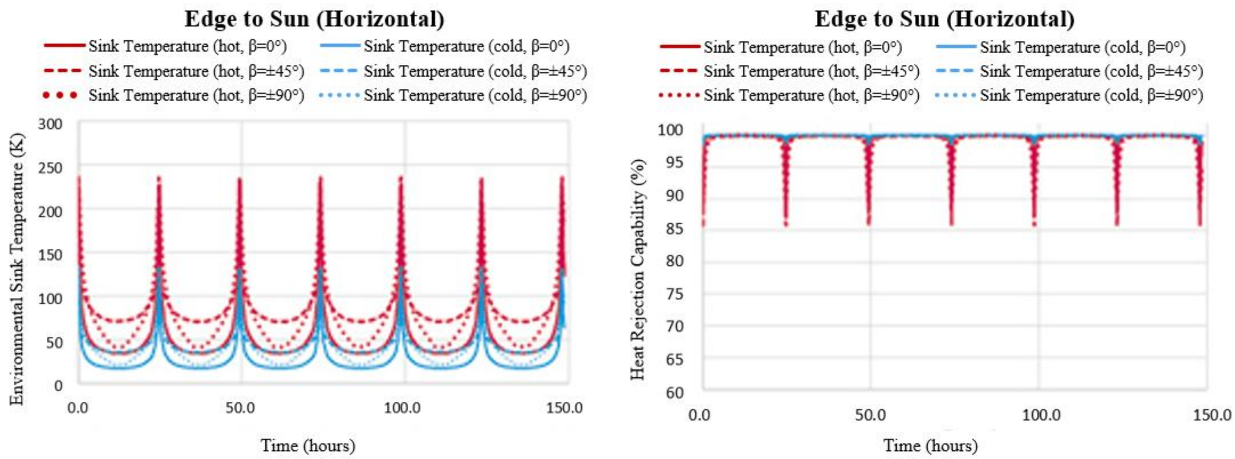

Figure 21. Six sequential Mars 1-Sol orbits.

Appendix D. Summary of Selected Cases.

Table 12 is a summary of all selected cases for this study. There are 35 cases selected in total.

Table 12. Summary of all selected cases.

Orbit	Specification	Reactor Power State	Panel Orientation	Case	± Beta Angle [°]	Case Number
LEO	500 km	OFF	Face to Earth (Edge to VV)	Hot	0	1
				Cold	52	2
			Face to Sun	Hot	0	3
				Cold	52	4
		ON	Edge to Sun (Vertical)	Hot	0	5
				Cold	52	6
	1100 km	OFF	Face to Earth (Edge to VV)	Hot	0	7
				Hot	52	8
				Cold	25	9
				Cold	52	10
			Face to Sun	Hot	0	11
				Hot	52	12
				Cold	25	13
				Cold	52	14
		ON	Edge to Sun (Vertical)	Hot	0	15
				Cold	52	16
NRHO	9:2 lunar synodic resonant, southern L2 Lagrangian point	OFF	Face to Sun	Hot	0	17
				Hot	45	18
				Cold	0	19
				Cold	45	20
		ON	Edge to Sun (Vertical)	Hot	0	21
				Hot	90	22
				Cold	0	23
Martian orbits	<1-Sol	ON	Edge to Sun (Horizontal)	Hot	45	24
				Cold	0	25
	1-Sol		Edge to Sun (Horizontal)	Hot	45	26
				Cold	0	27
	2-Sol		Edge to Sun (Horizontal)	Hot	45	28
				Cold	0	29
	5-Sol		Edge to Sun (Horizontal)	Hot	45	30
				Cold	0	31
	10-Sol		Edge to Sun (Horizontal)	Hot	45	32
				Cold	0	33
Venus flyby	Sample trajectory	ON	Edge to Sun (Horizontal)	Hot	45	34
				Cold	90	35

Table 13 and Table 14 summarize the selection of beta angles for modeling (from each of the selected panel orientations) for when the reactor is powered OFF and ON respectively. When the reactor is powered OFF, the objective is to maximize radiator panel temperature and prevent freezing. When the reactor is powered ON, the objective is to minimize radiator panel temperature, prevent overheating, and increase heat rejection. Environmental sink temperature for interplanetary space is included in the last row of Table 14 for comparison.

Given a range of beta angles studied for one panel orientation, the beta angle which observes the maximum or minimum T_∞ is identified and selected for future analysis. Other considerations for beta angle selection include lower or higher average T_∞, or longer/shorter duration in shadow when compared with other beta angles within that selected panel orientation.

Table 13. Reactor powered OFF: justification for beta angle selection and extrema of environmental sink temperature for selected panel orientations.

Location (Specification)	Case	Hot Case			Cold Case		
		± Beta angle	Justification for Beta Angle Selection	Maximum T_∞ [K]	± Beta angle	Justification for Selection	Minimum T_∞ [K]
LEO (500 km)	**01 – Face to Earth (Edge to VV)**	0˚	Maximum observed T_∞. Higher average T_∞.	**353**	52˚	Minimum observed T_∞. Lower T_∞ throughout orbit.	203
	04 – Face to Sun	0˚	Maximum observed T_∞. Higher average T_∞.	**353**	52˚	Minimum observed T_∞. Lower T_∞ throughout orbit.	188
LEO (1100 km)	**01 – Face to Earth (Edge to VV)**	0˚	Maximum observed T_∞. Higher average T_∞..	348	52˚	Lowest maximum T_∞ observed.	195
		52˚	Shortest duration in shadow.	316	25˚	Longer duration in shadow compared to 52˚ case. Lower average T_∞ compared to 0˚ case.	195
	04 – Face to Sun	0˚	Maximum observed T_∞. Higher average T_∞.	348	52˚	Minimum observed T_∞. Lower T_∞ throughout orbit.	176
		52˚	Shortest duration in shadow.	335	25˚	Longer duration in shadow compared to 52˚ case. Lower average T_∞ compared to 0˚ case.	190
NRHO (9:2 lunar synodic resonant, southern L2 Lagrangian point)	**04 – Face to Sun**	0˚	Maximum observed T_∞.	328	0˚	Minimum observed T_∞. Vehicle passes through shadow.	**30**
		45˚	Higher average T_∞. Vehicle avoids shadow.	325	90˚	Lower T_∞ throughout orbit. Vehicle avoids shadow.	312

Worst case hot	**Worst case cold**

Table 14. Reactor powered ON: justification for beta angle selection and extrema of environmental sink temperature for selected panel orientations.

Orbit (Specification)	Orientation	Hot Case			Cold Case		
		± Beta angle	Justification for Selection	Maximum T_∞ [K]	± Beta angle	Justification for Selection	Minimum T_∞ [K]
LEO (500 km)	**05 – Edge to Sun (Vertical)**	0˚	Maximum observed T_∞. Higher average T_∞.	239	52˚	Minimum observed T_∞. Lower average T_∞.	180
LEO (1100 km)	**05 – Edge to Sun (Vertical)**	0˚	Maximum observed T_∞. Higher average T_∞.	220	52˚	Minimum observed T_∞. Lower average T_∞.	164
NRHO (9:2 lunar synodic resonant, southern L2 Lagrangian point)	**06 – Edge to Sun (Vertical)**	90˚	Higher T_∞ throughout orbit.	163	0˚	Minimum observed T_∞. Lower average T_∞. Vehicle passes through shadow.	13
		0˚	Largest temperature gradient.	146			
Mars orbit (<1-Sol)	**05 – Edge to Sun (Horizontal)**	45˚	Maximum observed T_∞. Higher average T_∞.	**243**	0˚	Minimum observed T_∞. Lower average T_∞.	43
Mars orbit (1-Sol)	**05 – Edge to Sun (Horizontal)**	45˚	Maximum observed T_∞. Higher average T_∞.	**243**	0˚	Minimum observed T_∞. Lower average T_∞.	17
Mars orbit (2-Sol)	**05 – Edge to Sun (Horizontal)**	45˚	Maximum observed T_∞. Higher average T_∞.	**243**	0˚	Minimum observed T_∞. Lower average T_∞..	12
Mars orbit (5-Sol)	**05 – Edge to Sun (Horizontal)**	45˚	Maximum observed T_∞. Higher average T_∞.	**243**	0˚	Minimum observed T_∞. Lower average T_∞..	7
Mars orbit (10-Sol)	**05 – Edge to Sun (Horizontal)**	45˚	Maximum observed T_∞. Higher average T_∞.	**243**	0˚	Minimum observed T_∞. Lower average T_∞.	5
Venus flyby (altitude model, 6000 km)	**05 – Edge to Sun (Horizontal)**	45˚	Maximum observed T_∞.	221	90˚	Minimum observed T_∞.	118
For Comparison:							
Interplanetary Space	**Edge to Sun**	N/A	N/A	N/A	N/A	N/A	**2.7**

Worst case hot	**Worst case cold**

Appendix E. All Environmental Sink Temperature and Heat Rejection Capability Curves

LEO 500 km

Environmental Sink Temperature

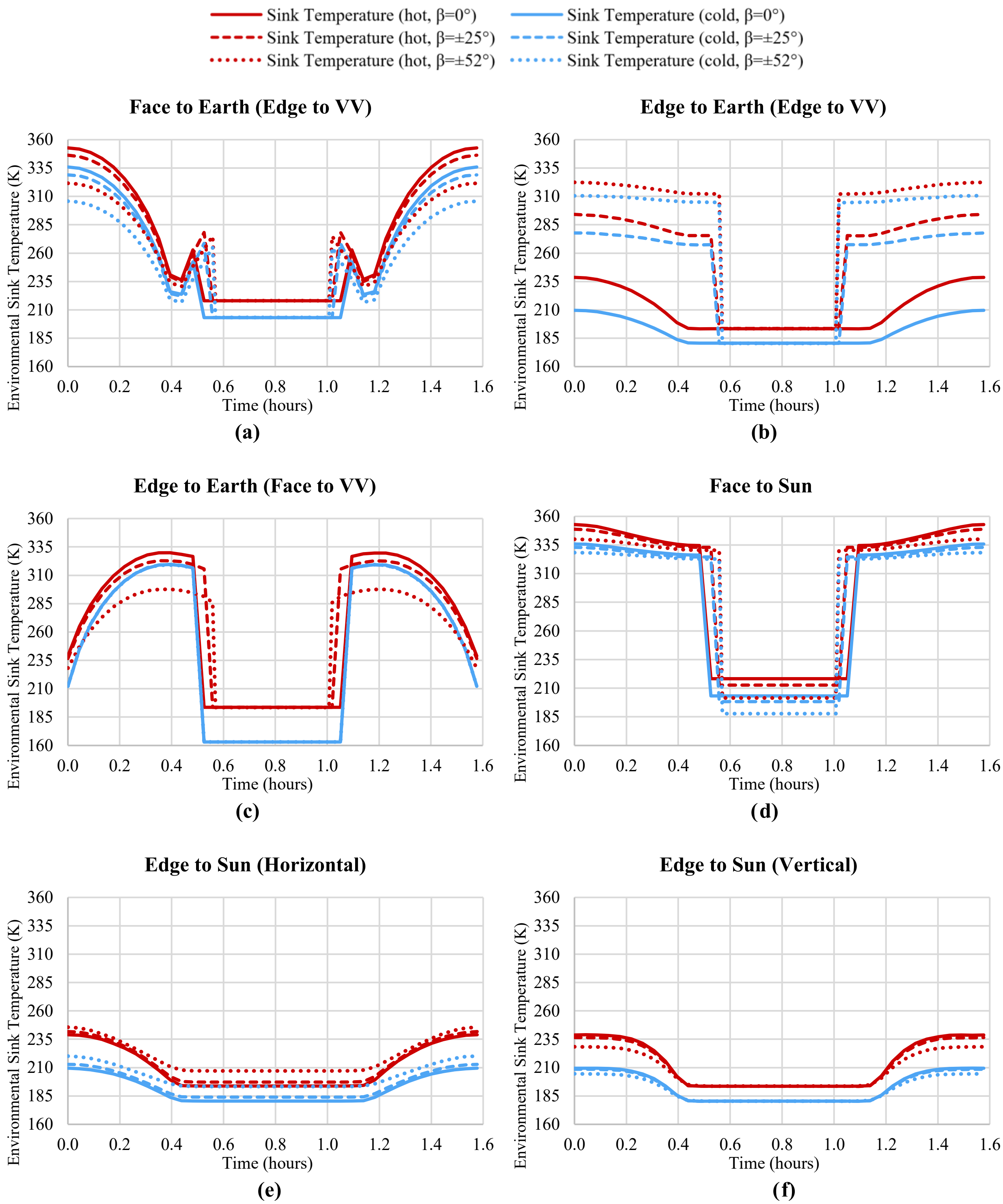

Figure 22. Hot and cold case environmental sink temperature curves for LEO 500 km. Orbital period: ~1.58 hours.

Low Earth Orbit (500 km)

Heat Rejection Capability

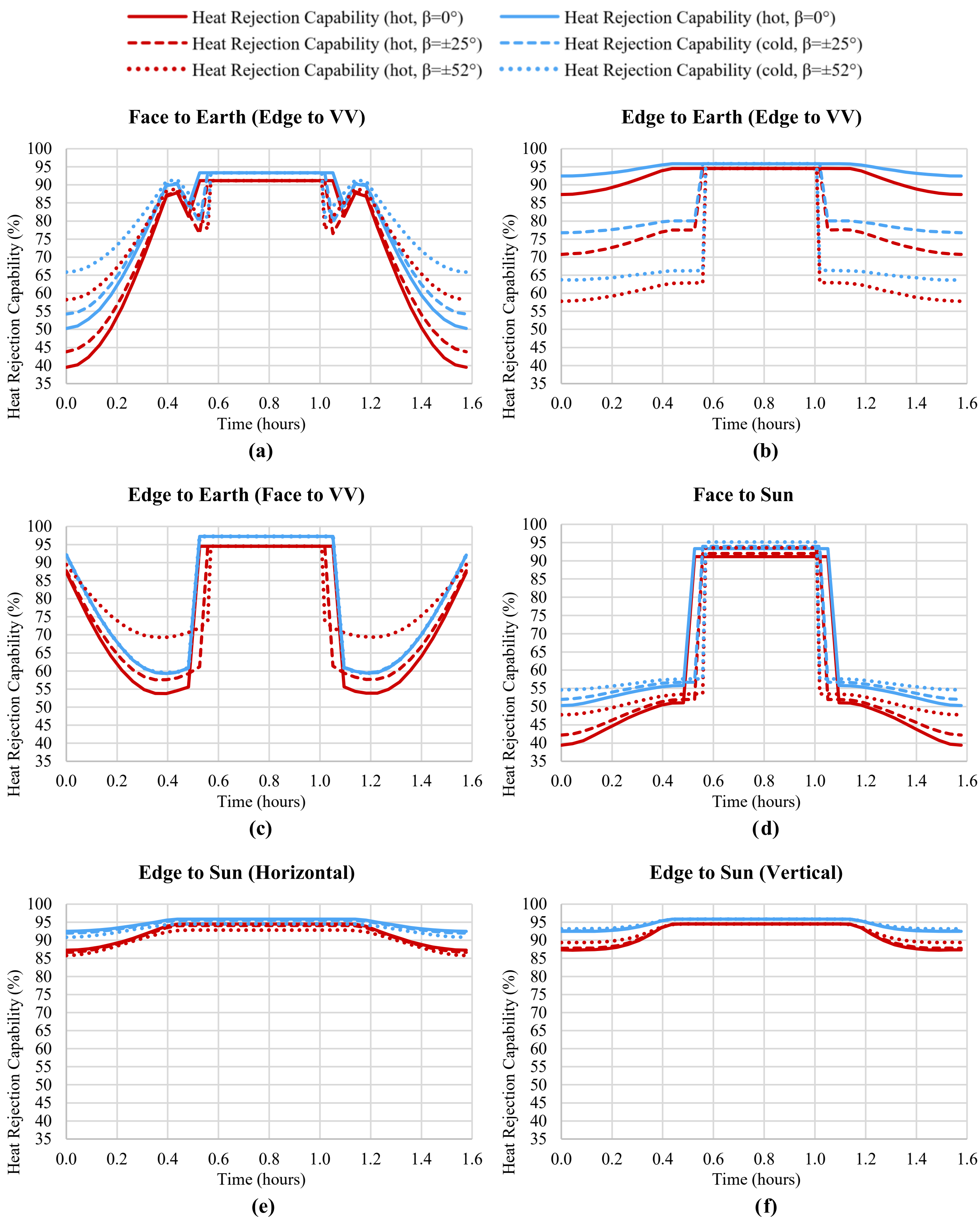

Figure 23. Hot and cold case heat rejection capability curves for LEO 500 km. Orbital period: ~1.58 hours.

Low Earth Orbit (1100 km)

Environmental Sink Temperature

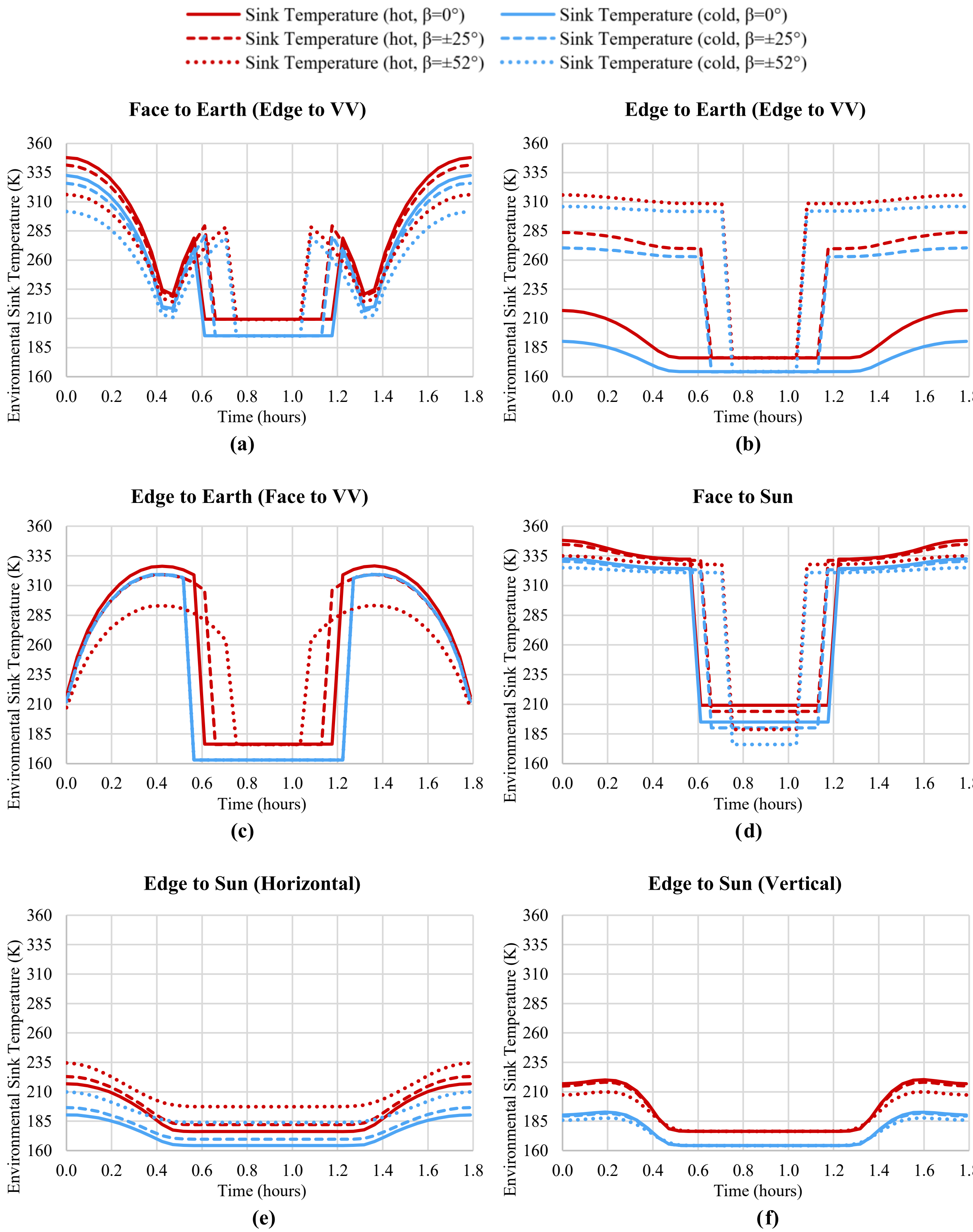

Figure 24. Hot and cold case environmental sink temperature curves for LEO 1100 km. Orbital period: ~1.79 hours.

Low Earth Orbit (1100 km)

Heat Rejection Capability

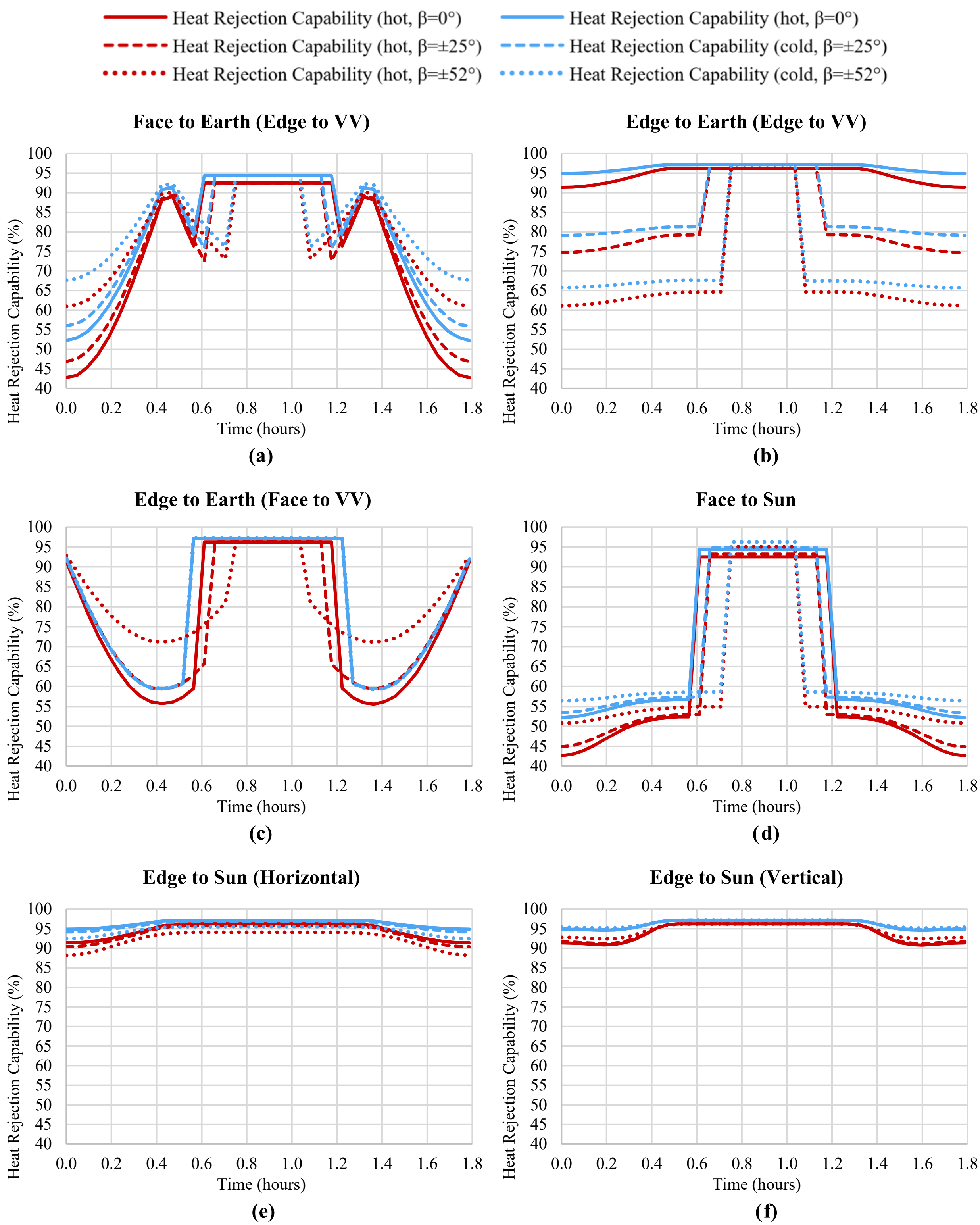

Figure 25. Hot and cold case heat rejection capability curves for LEO 1100 km. Orbital period: ~1.79 hours.

Near-Rectilinear Halo Orbit – 9:2 Lunar Synodic Resonant, Southern L2 Lagrangian Point

Environmental Sink Temperature

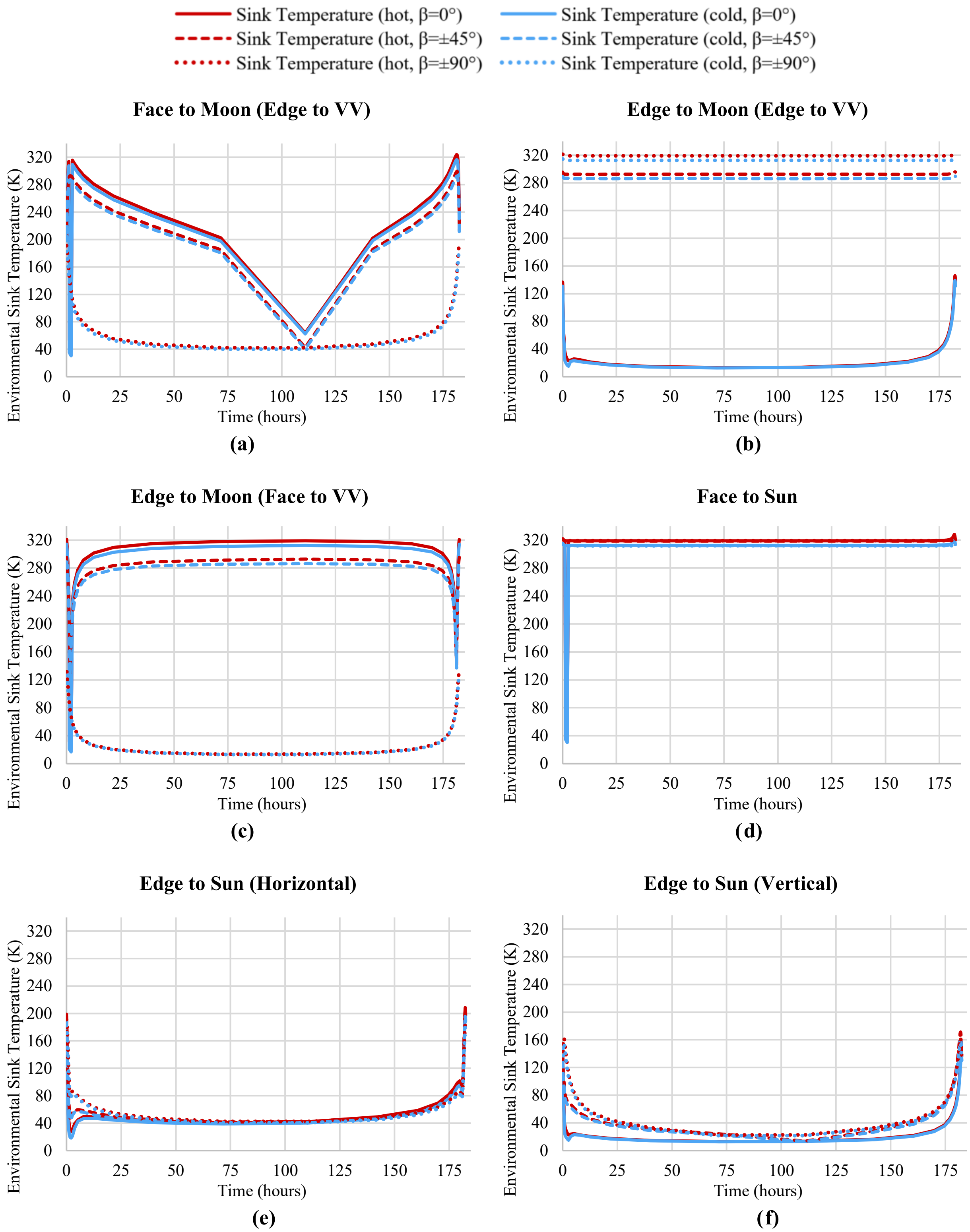

Figure 26. Hot and cold case environmental sink temperature curves for Gateway NRHO. Orbital period: 182.5 hours.

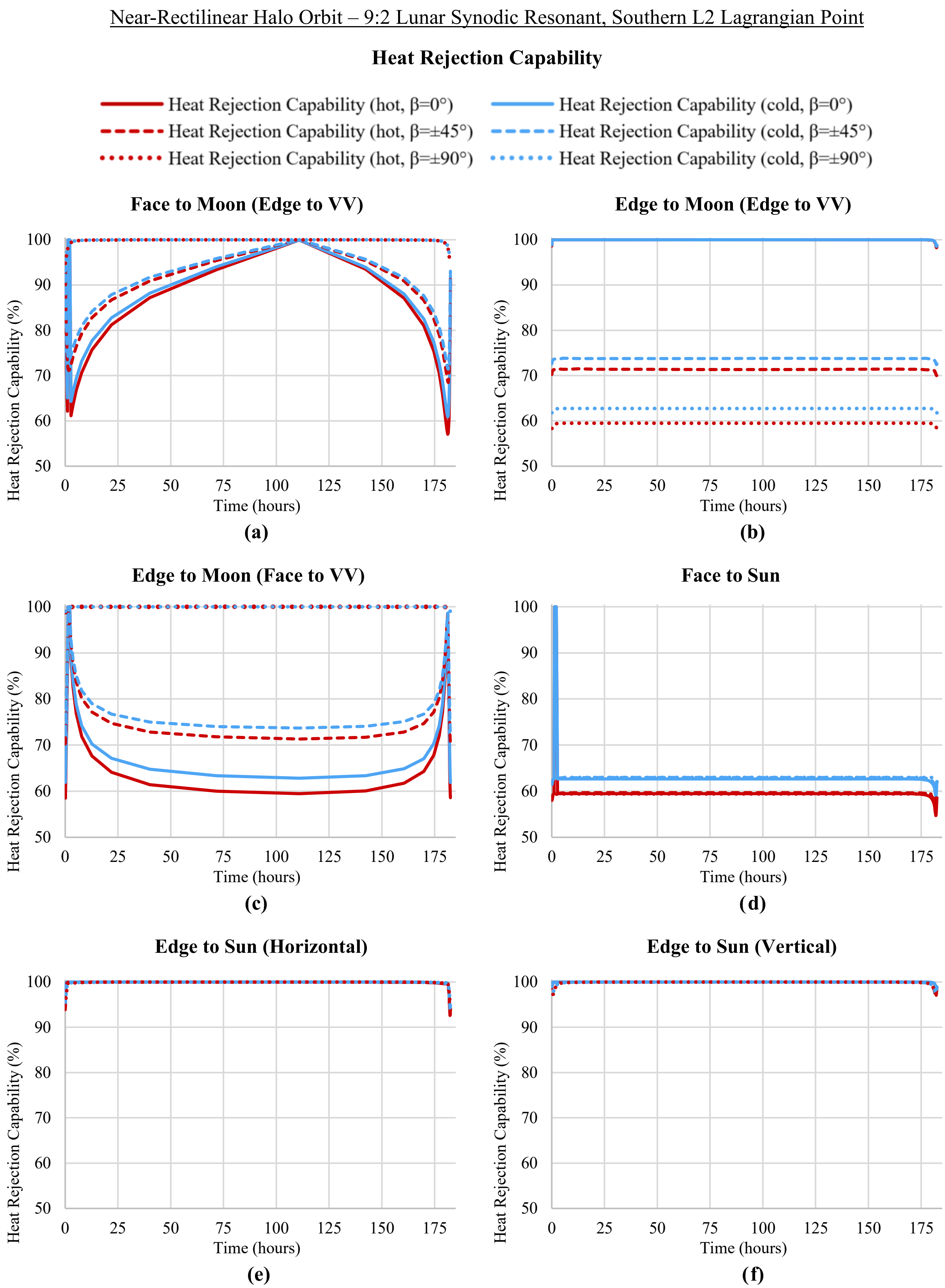

Figure 27. Hot and cold case heat rejection capability curves for Gateway NRHO. Orbital period: ~182.5 hours.

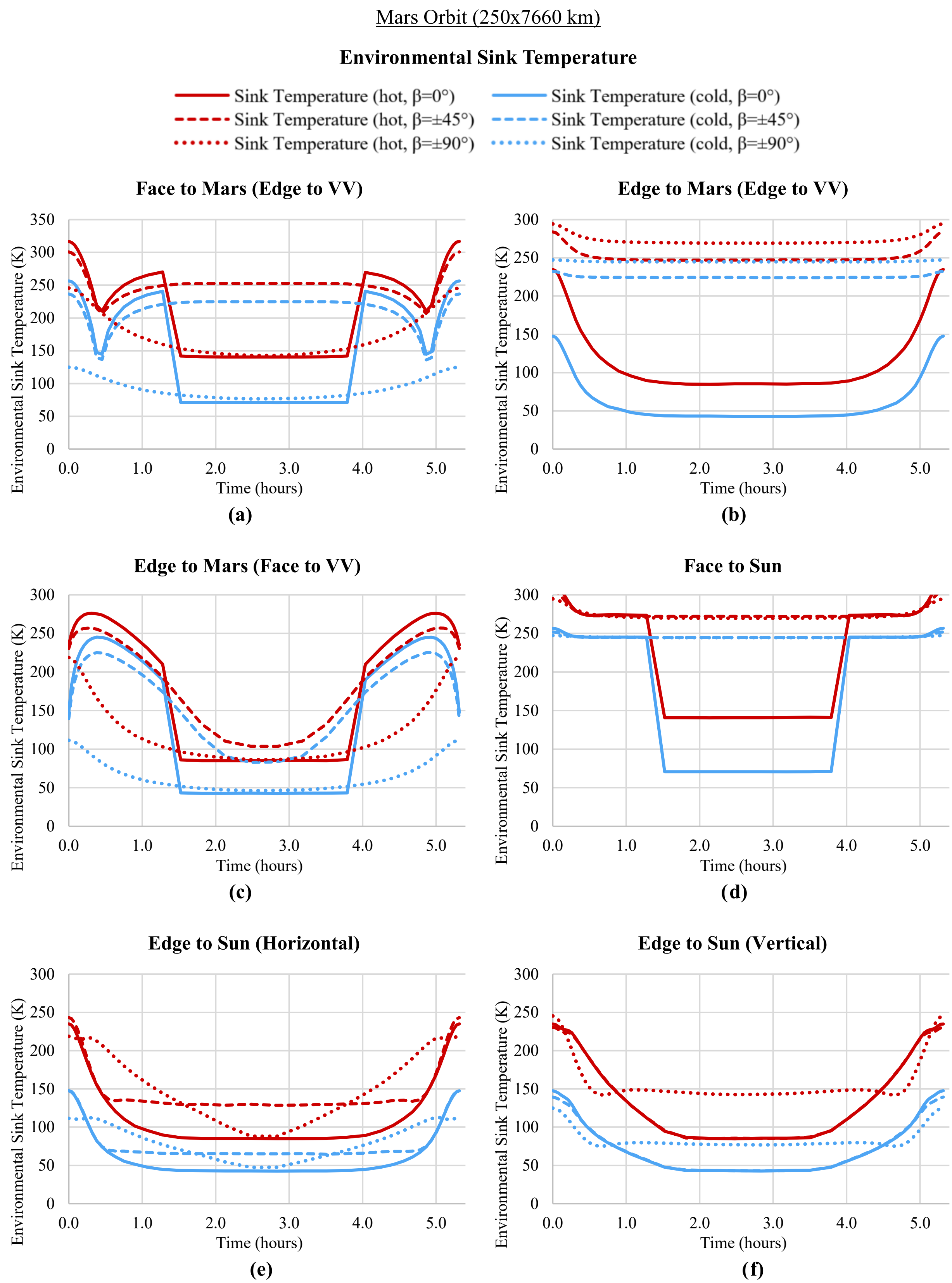

Figure 28. Hot and cold case environmental sink temperature curves for 250x7660 km Mars orbit. Orbital period: ~5.3 hours.

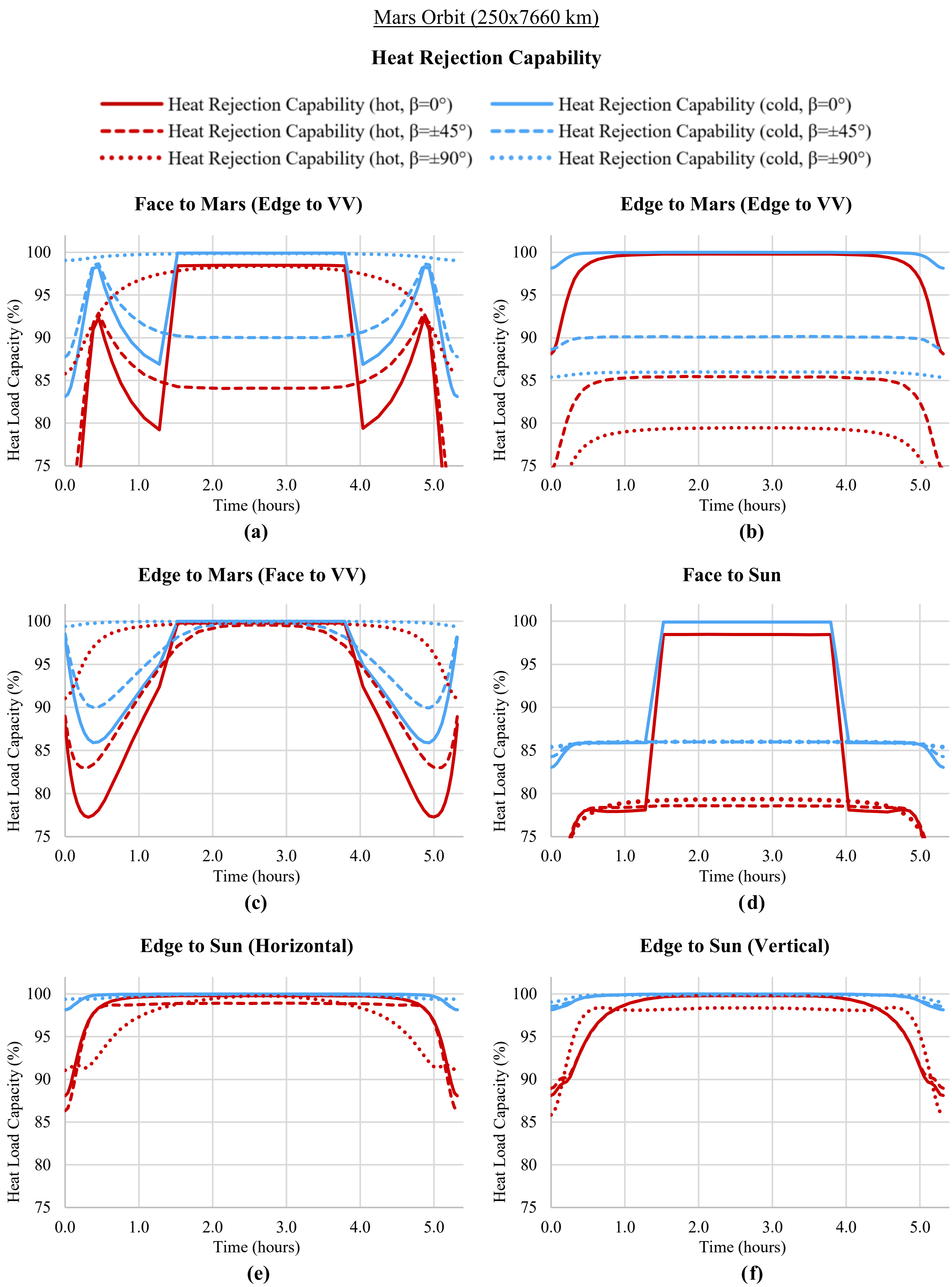

Figure 29. Hot and cold case heat rejection capability curves for 250x7660 km Mars orbit. Orbital period: ~5.3 hours.

Mars Orbit (1-Sol)

Environmental Sink Temperature

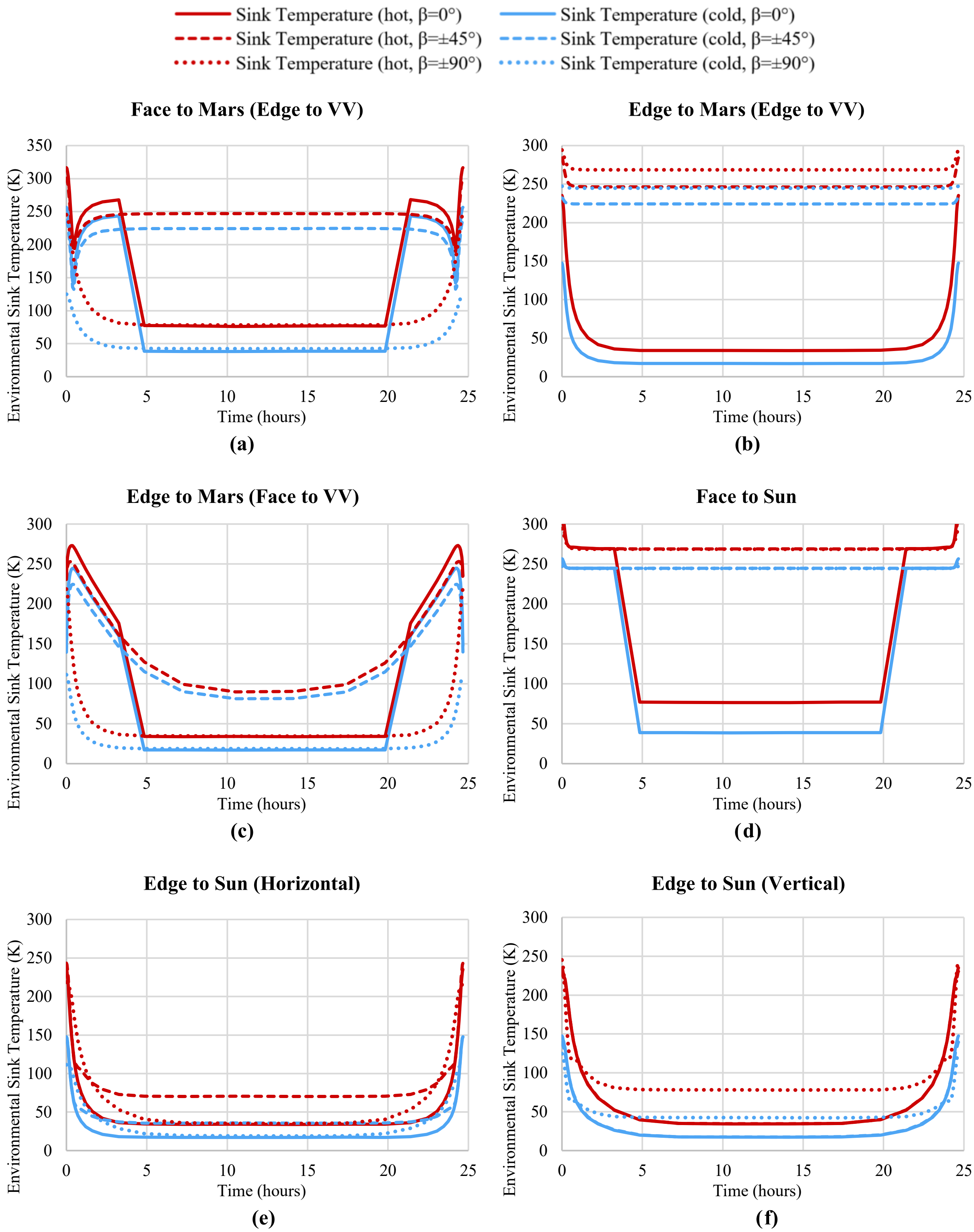

Figure 30. Hot and cold case environmental sink temperature curves for 1-Sol Mars orbit. Orbital period: 1-Sol or ~24.7 hours.

Mars Orbit (1-Sol)

Heat Rejection Capability

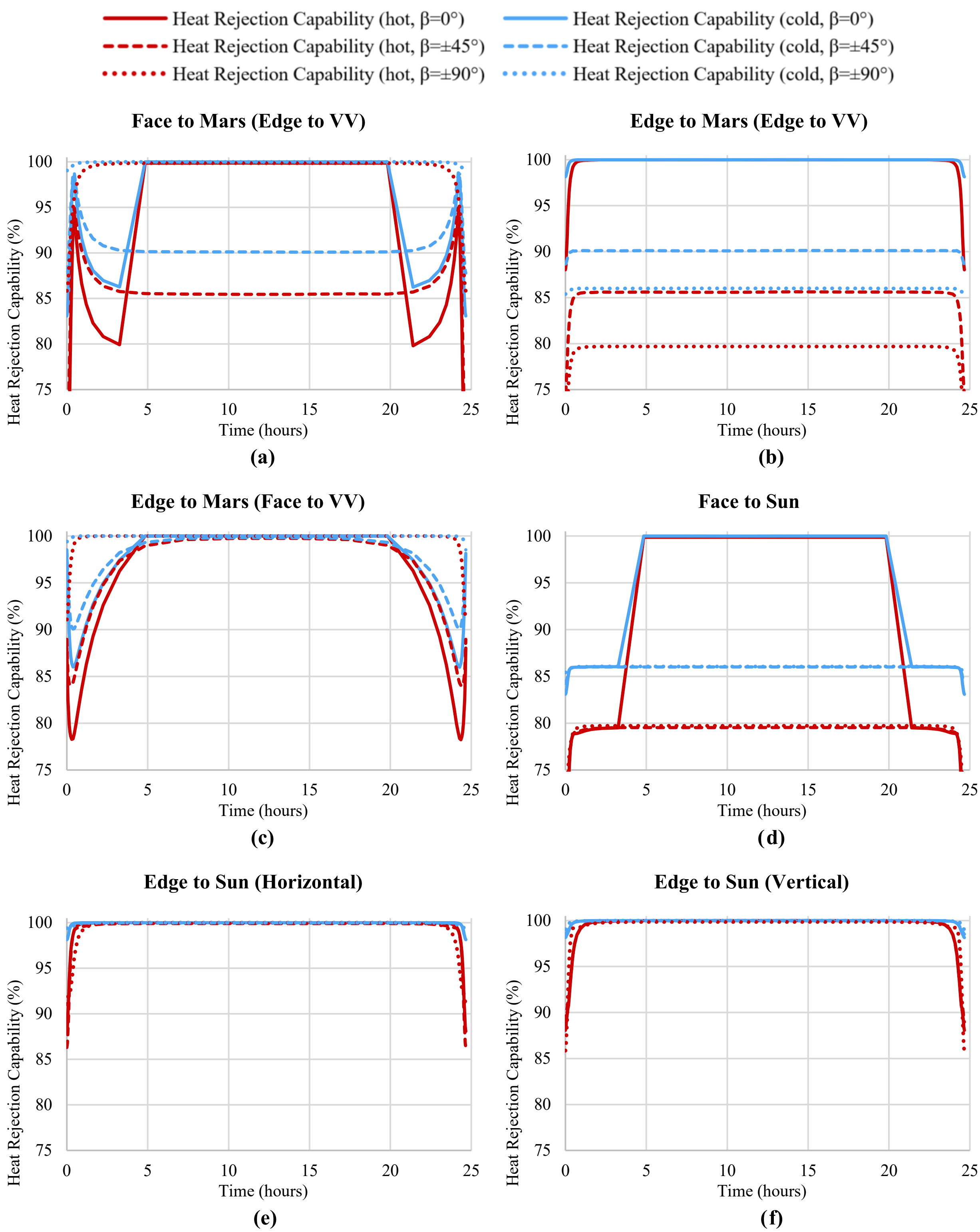

Figure 31. Hot and cold case heat rejection capability curves for 1-Sol Mars orbit. Orbital period: 1-Sol or ~24.7 hours.

Mars Orbit (2-Sol)

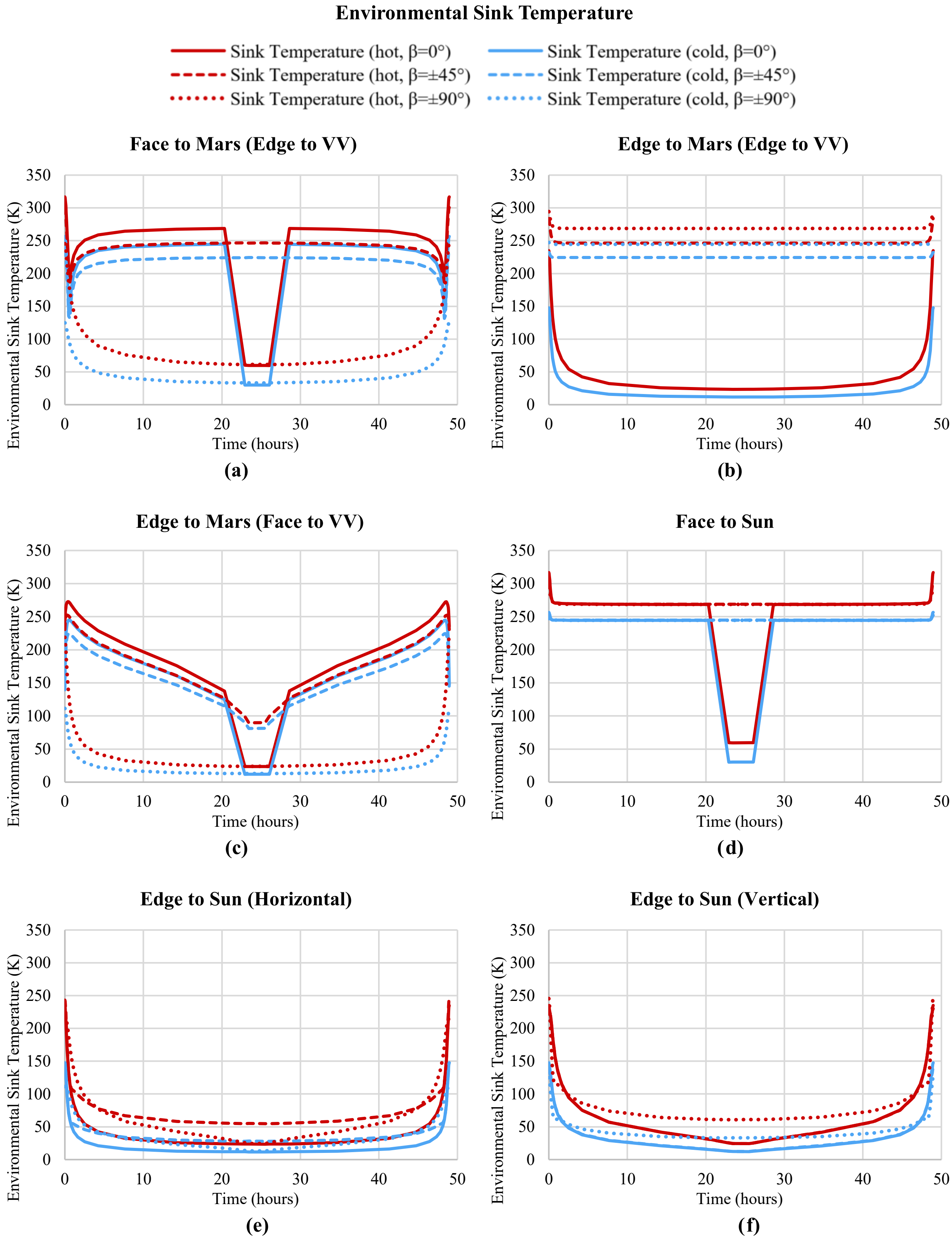

Figure 32. Hot and cold case environmental sink temperature curves for 2-Sol Mars orbit. Orbital period: 2-Sol or ~49 hours.

Mars Orbit (2-Sol)

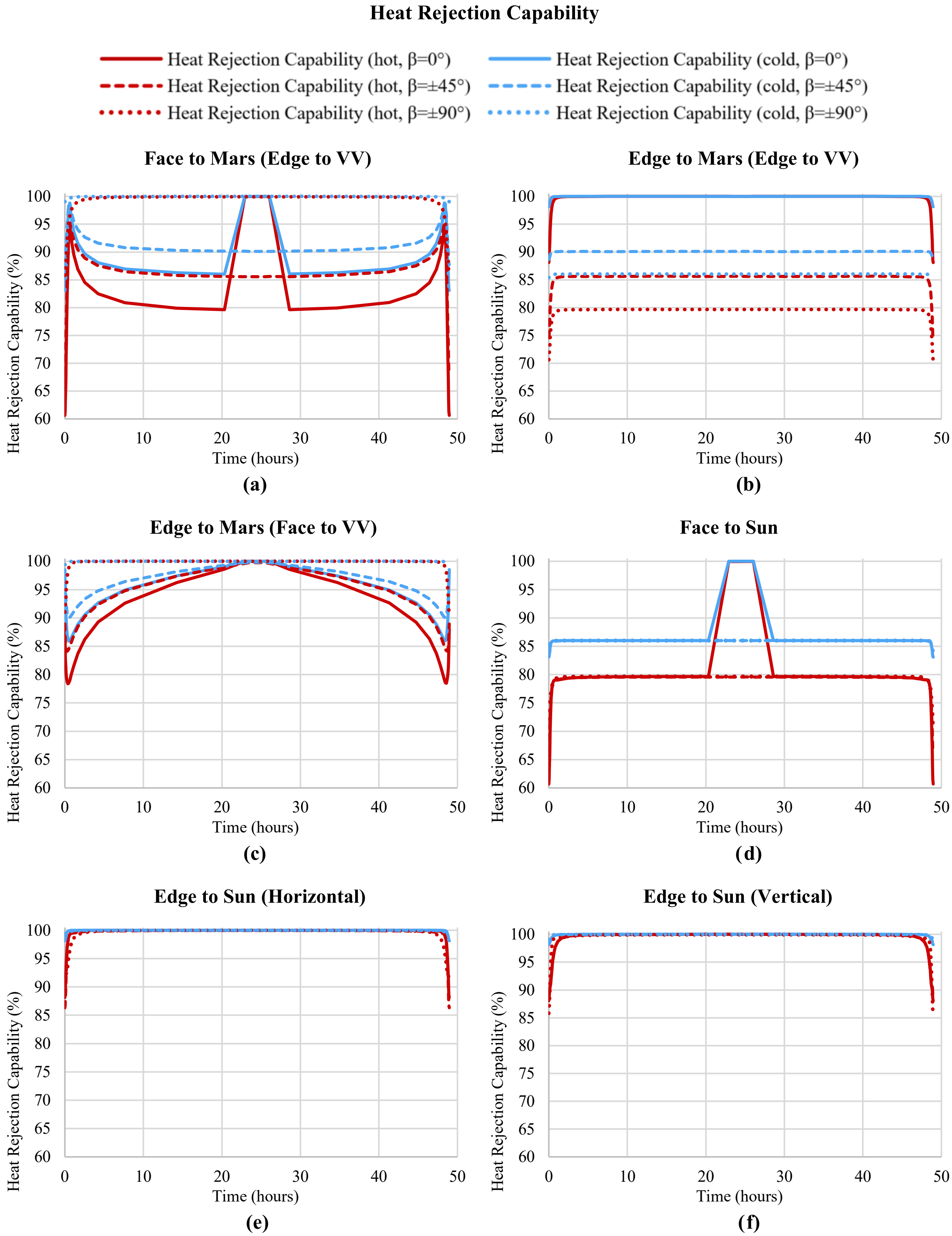

Figure 33. Hot and cold case heat rejection capability curves for 2-Sol Mars orbit. Orbital period is 2-Sol or ~49 hours.

Mars Orbit (5-Sol)

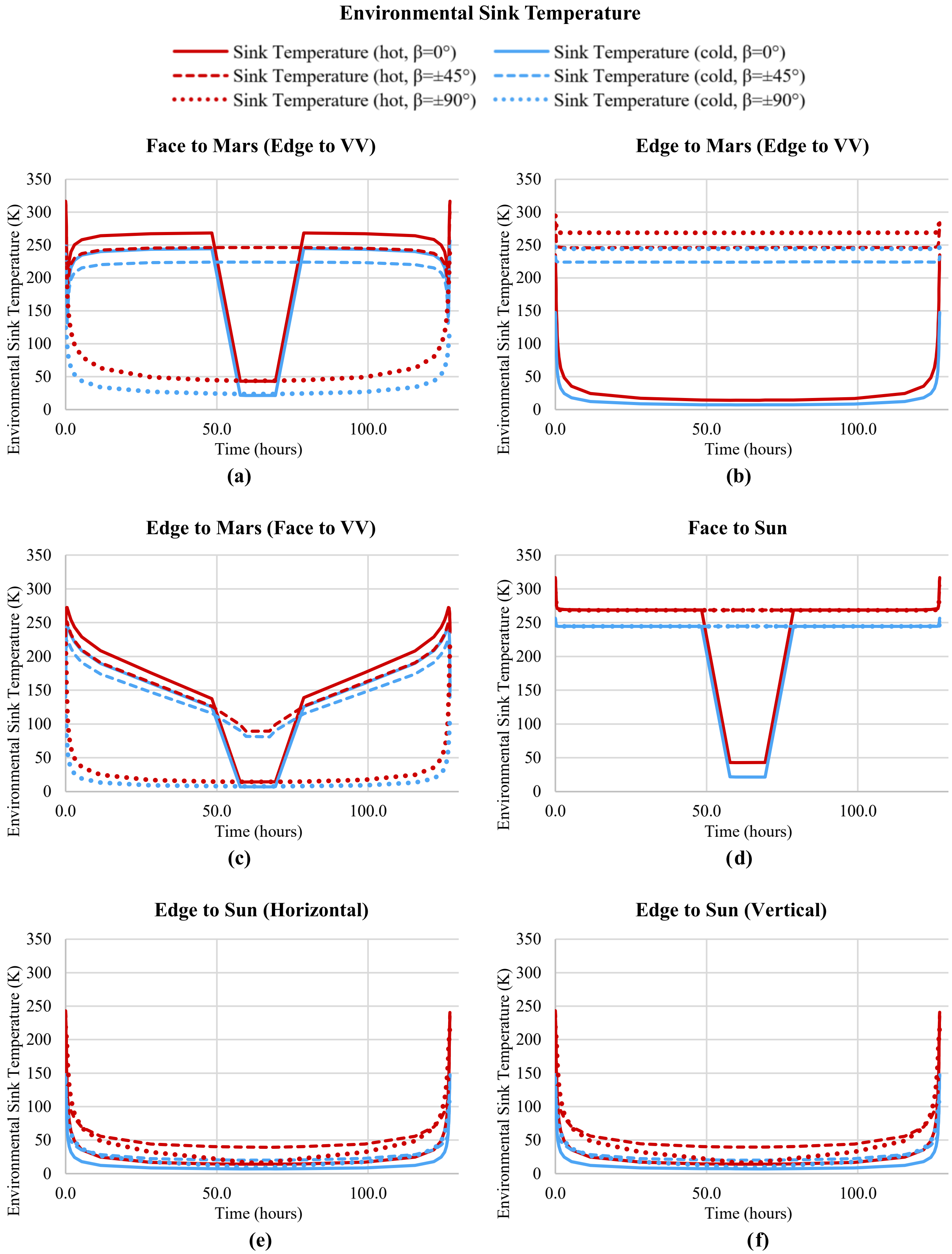

Figure 34. Hot and cold case environmental sink temperature curves for 5-Sol Mars orbit. Orbital period: 5-Sol or ~127 hours.

Mars Orbit (5-Sol)

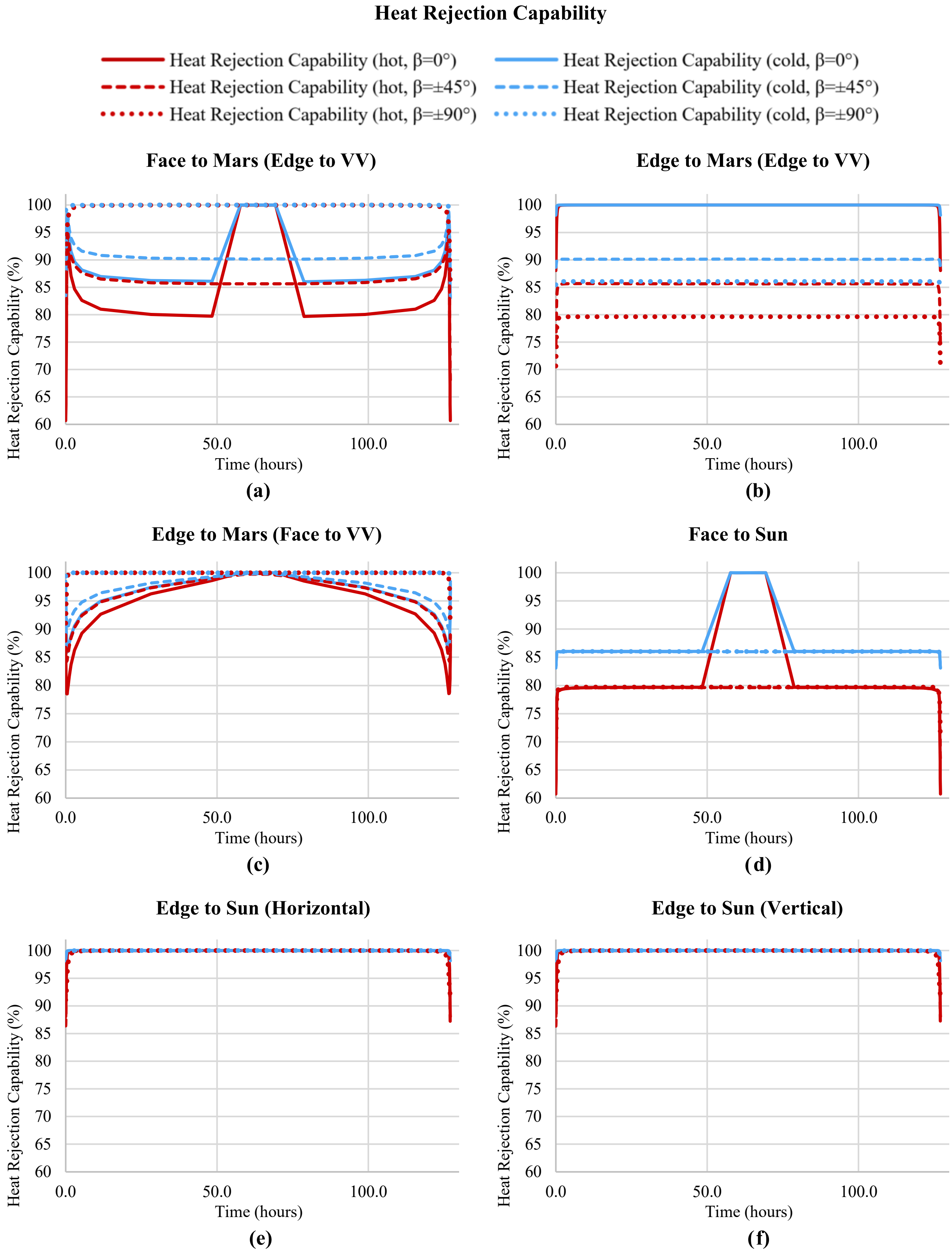

Figure 35. Hot and cold case heat rejection capability curves for 5-Sol Mars orbit. Orbital period: 5-Sol or ~127 hours.

Mars Orbit (10-Sol)

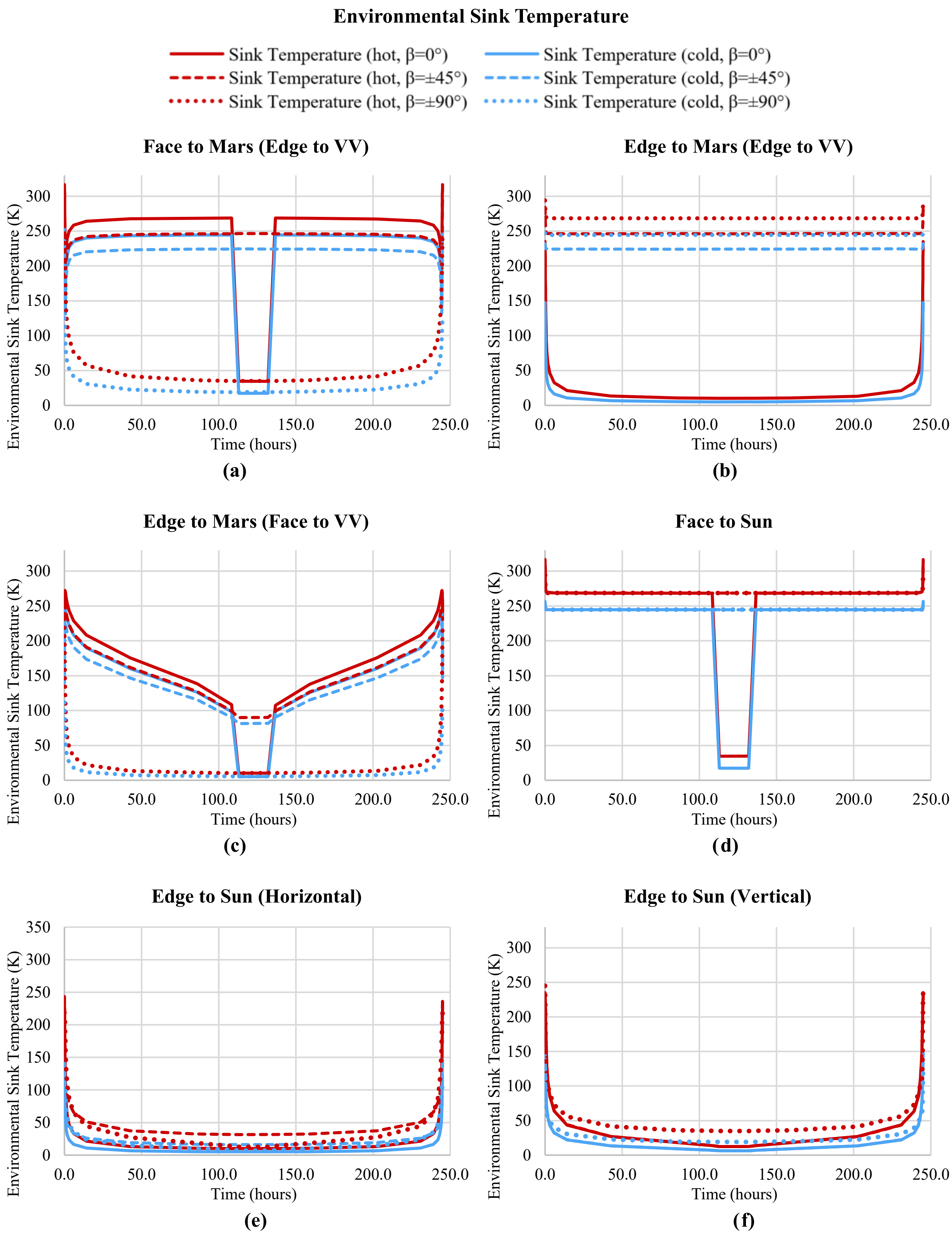

Figure 36. Hot and cold case environmental sink temperature curves for 10-Sol Mars orbit. Orbital period: 10-Sol or ~245 hours.

Mars Orbit (10-Sol)

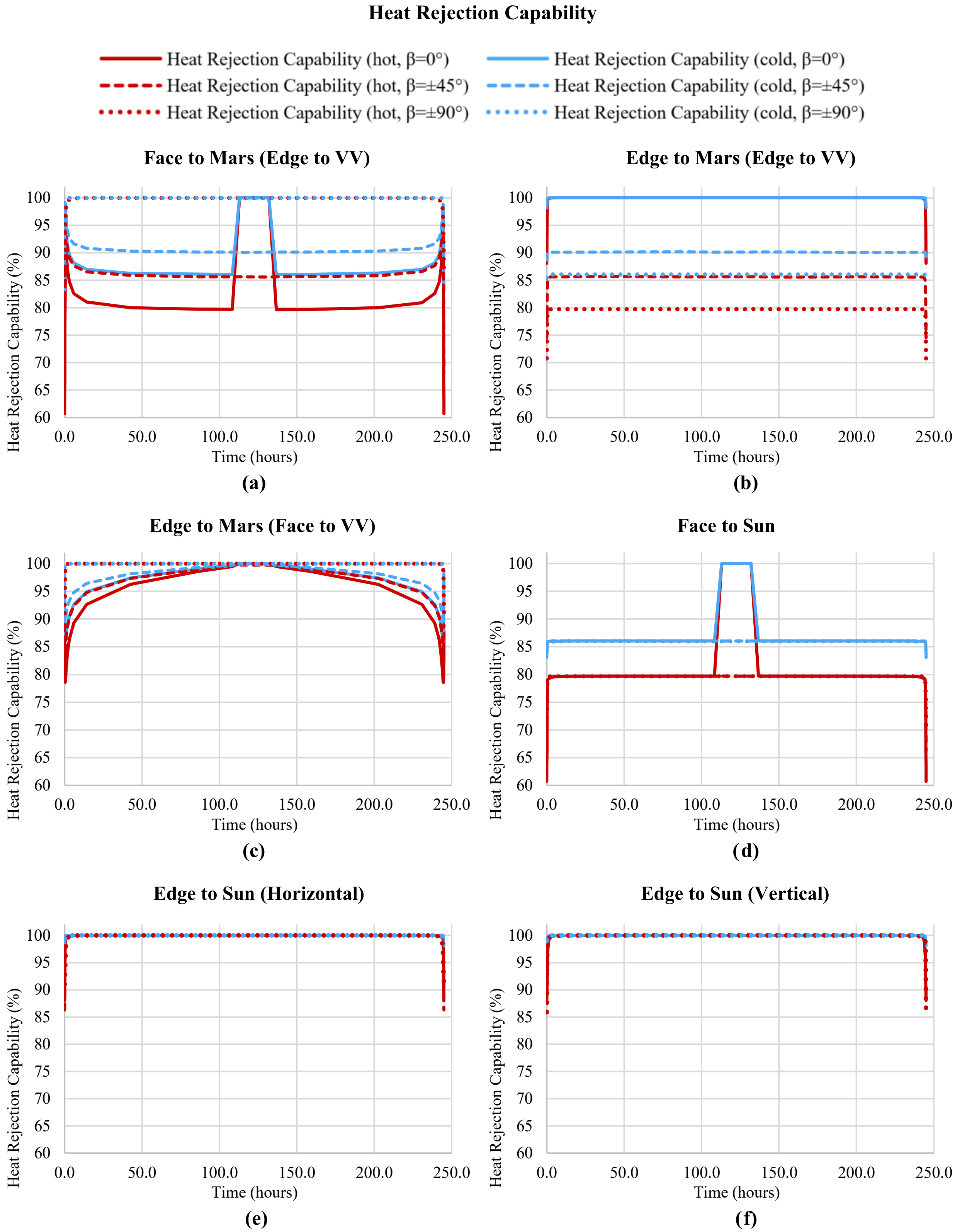

Figure 37. Hot and cold case heat rejection capability curves for 10-Sol Mars orbit. Orbital period: 10-Sol or ~245 hours.

Venus Flyby (Finite Altitude Positions Model)

Environmental Sink Temperature

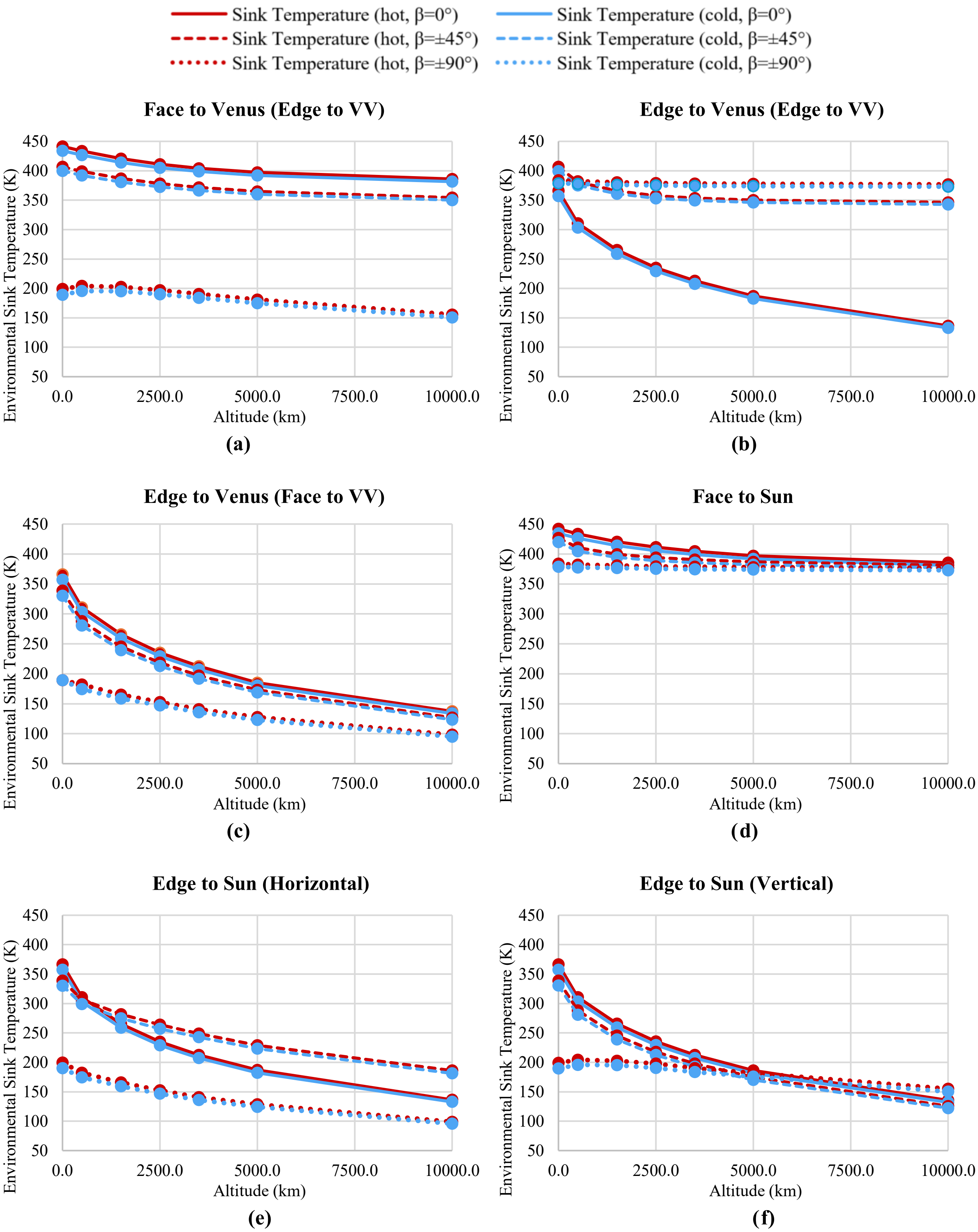

Figure 38. Hot and cold case environmental sink temperature curves for Venus flyby finite altitude positions model.

Venus Flyby (Finite Altitude Positions Model)

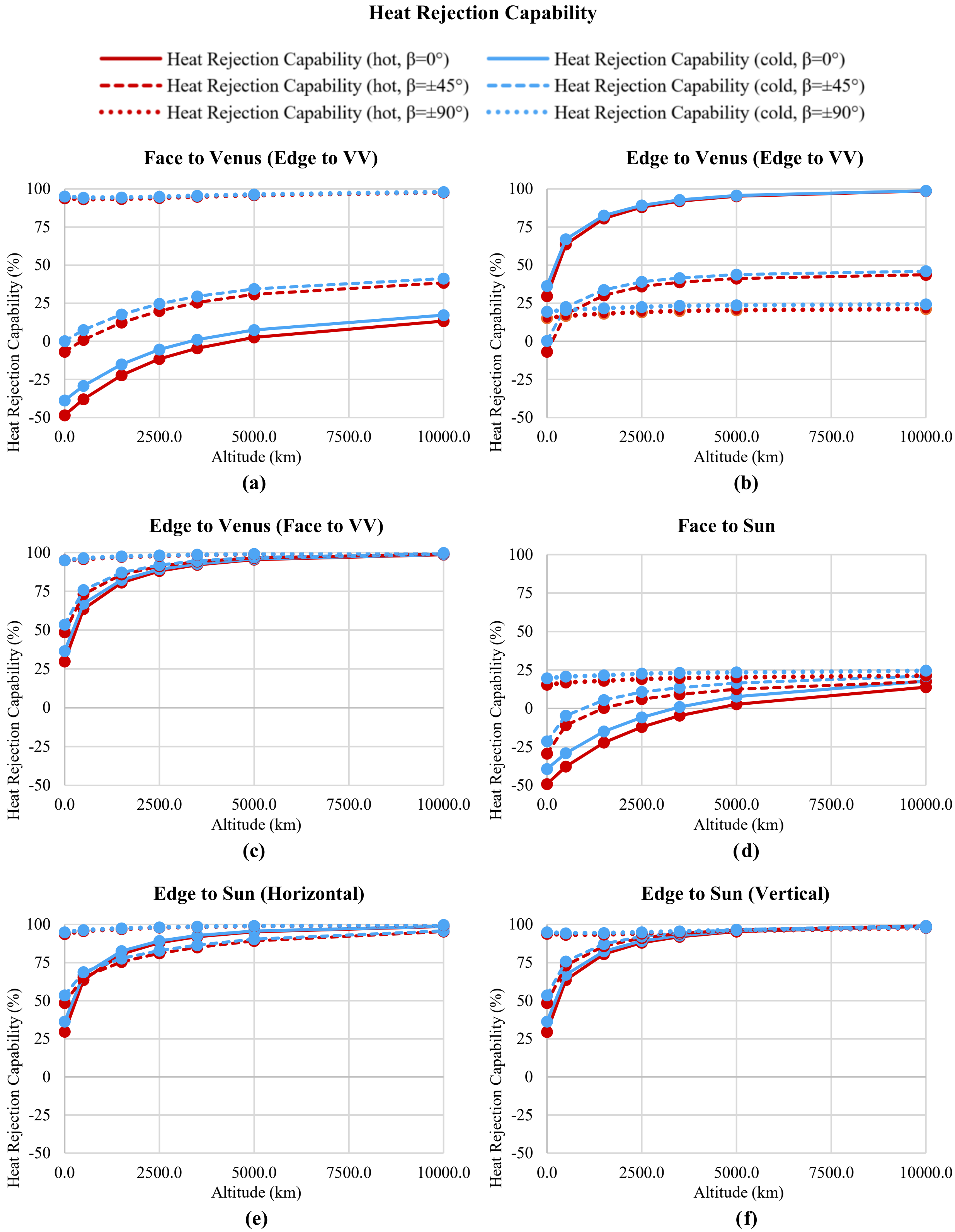

Figure 39. Hot and cold case heat rejection capability curves for Venus flyby finite altitude positions model.

Venus Flyby (Sample Trajectory)

Environmental Sink Temperature

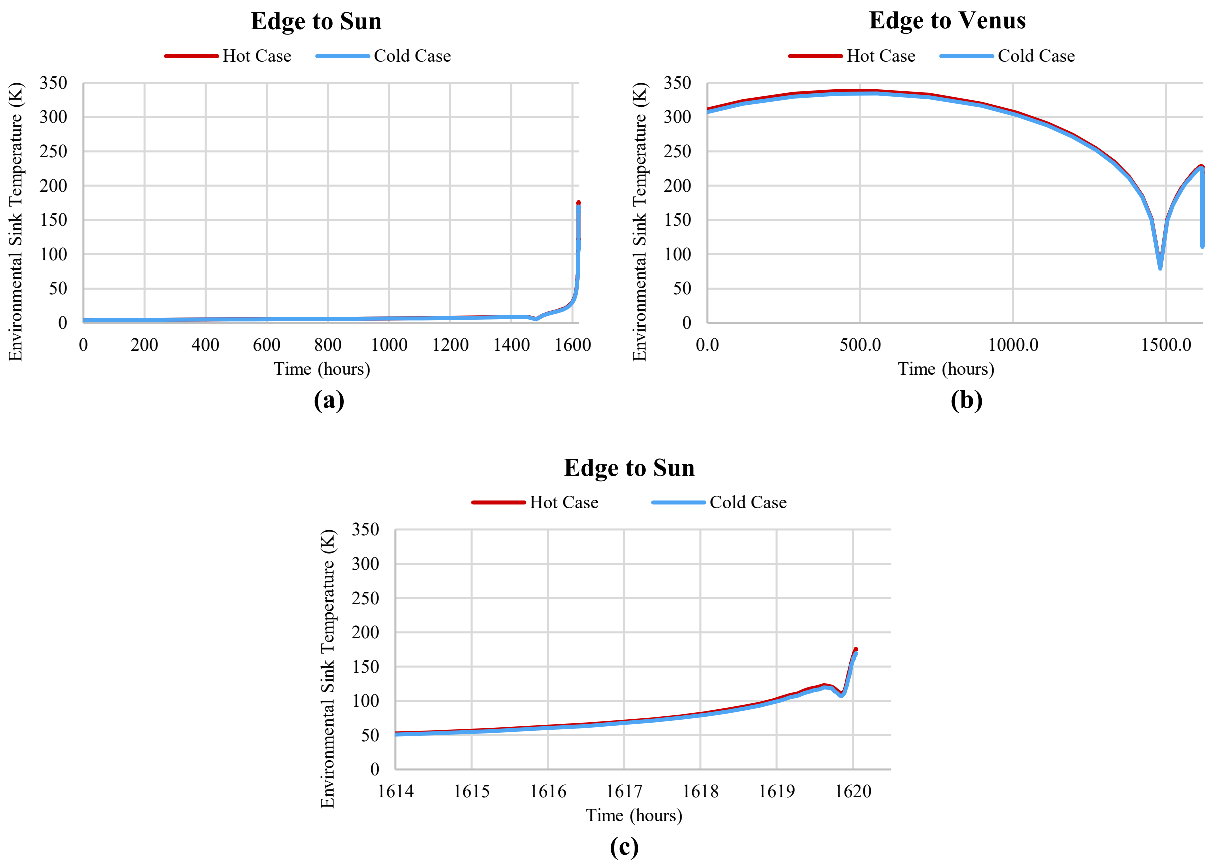

Figure 40. (a) (b) Hot and cold case environmental sink temperature curves for Venus flyby (sample trajectory). (c) Detailed view of "edge to Sun" orientation near end of sample trajectory.

Heat Rejection Capability

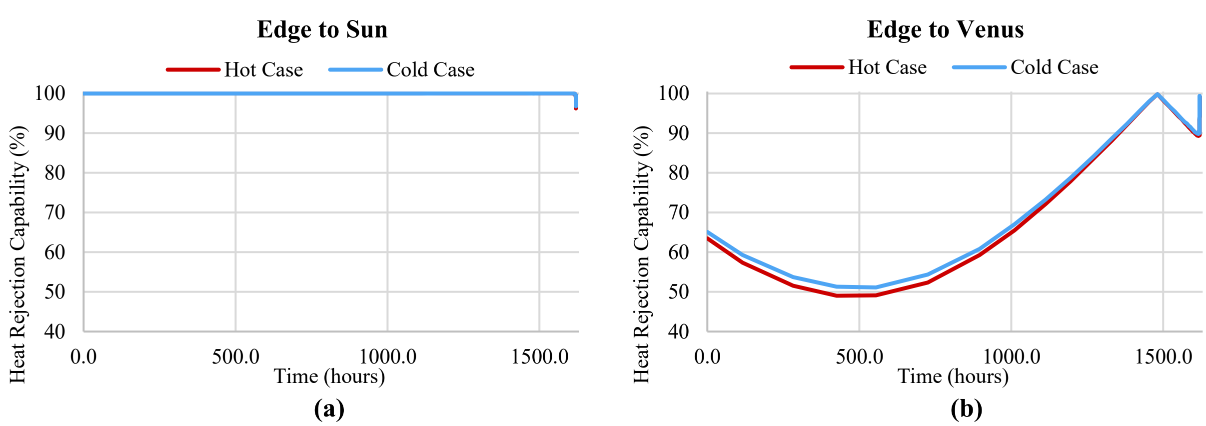

Figure 41. Hot and cold case heat rejection capability curves for Venus flyby (sample trajectory).